DIMINISHED TEMPERATURE AND VEGETATION SEASONALITY OVER NORTHERN HIGH LATITUDES

L. Xu,[1]* R. B. Myneni,[1]* F. S. Chapin III,[2] T. V. Callaghan,[3,4] J. E. Pinzon,[5] C. J. Tucker,[5] Z. Zhu[1], J. Bi[1], P. Ciais,[6] H. Tømmervik,[7] E. S. Euskirchen,[2] B. C. Forbes,[8] S.L. Piao,[9,10] B.T. Anderson,[1] S. Ganguly,[11] R. R. Nemani,[12] S. J. Goetz,[13] P. S. A. Beck,[13] A. G. Bunn,[14] C. Cao,[15,16] J. C. Stroeve[17]

[1]Department of Earth and Environment, Boston University, Boston, MA 02215, USA

[2]Institute of Arctic Biology, University of Alaska Fairbanks, Fairbanks, AK 99775, USA

[3]Royal Swedish Academy of Sciences, PO Box 50005, 104 05 Stockholm, Sweden.

[4]Department of Animal and Plant Sciences, University of Sheffield, Western Bank, Sheffield, S10 2TN, UK

[5]Biospheric Sciences Branch, NASA Goddard Space Flight Center, Greenbelt, MD 20771, USA

[6]Laboratoire des Sciences du Climat et de l'Environnement, CEA-CNRS-UVSQ ; 91191 Gif sur Yvette, Cedex, France

[7]Norwegian Institute for Nature Research, Fram-High North Research Center for Climate and the Environment, N-9296, Tromsø, Norway

[8]Arctic Centre, University of Lapland, Rovaniemi, FI-96101, Finland

[9]Department of Ecology, Peking University, Beijing 100871, China.

[10]Institute of Tibetan Plateau Research, Chinese Academy of Sciences, Beijing 100085, China

[11]Bay Area Environmental Research Institute, NASA Ames Research Center, Moffett Field, CA 94035, USA

[12]NASA Advanced Supercomputing Division, Ames Research Center, Moffett Field, CA 94035, USA

[13]The Woods Hole Research Center, Woods Hole, Falmouth, MA 02540, USA

[14]Department of Environmental Sciences, Huxley College, Western Washington University, Bellingham, WA 98225, USA

[15]State Key Laboratory of Remote Sensing Science, Institute of Remote Sensing and Digital Earth, Chinese Academy of Sciences, Beijing 100101, China

[16]School of Resources and Environment, University of Electronic Science and Technology of China, Chengdu, Sichuan, 611731, China

[17]National Snow and Ice Data Center, University of Colorado, Boulder, CO 80309, USA

*These authors contributed equally to this work.

Contents

1

Abbreviations

ADF	Augmented Dickey-Fuller Test
AIC	Akaike Information Criterion
AR	Auto-Regressive
AVHRR	Advanced Very High Resolution Radiometer
ARIMA	Auto-Regressive Integrated Moving Average
CAVM	Circumpolar Arctic Vegetation Map
CCSM4	Community Climate System Model 4
CMIP5	Coupled Model Intercomparison Project 5
CPC	Climate Prediction Center
CRU	Climate Research Unit, University of East Anglia, UK
CRUTEM4	CRU 5° by 5° temperature data
FWSM	Full Width at Sixth of Maximum
GIMMS	Global Inventory Modeling and Mapping Studies
GISS	Goddard Institute for Space Studies (NASA)
IGBP	International Geosphere-Biosphere Programme
MA	Moving Average
MODIS	Moderate Resolution Imaging Spectroradiometer
NASA	National Aeronautics and Space Administration
NCAR	National Center for Atmospheric Research
NCEP	National Centers for Environmental Prediction
NDVI	Normalized Difference Vegetation Index
NDVIg	Version of GIMMS NDVI previous to NDVI3g
NDVI3g	Third Generation of AVHRR GIMMS NDVI
NOAA	National Oceanic and Atmospheric Administration
NSIDC	National Snow and Ice Data Center
OLS	Ordinary Least Squares
PAP	Photosynthetically Active Period
pdfs	Probability Density Functions
RCP 8.5	Representative Concentration Pathway 8.5
RMSE	Root Mean Square Error
SeaWiFS	Sea-Viewing Wide-Field-of-View Sensor
SE	Standard Error
SLT	Simple Linear Trend Model
SPOT	Satellite Pour l'Observation de la Terre

2

S1. Supplementary Data

S1.A. AVHRR NDVI Data

The latest version (third generation) of the Normalized Difference Vegetation Index (GIMMS NDVI3g) data set generated from the Advanced Very High Resolution Radiometers (AVHRR) onboard a series of NOAA satellites (NOAA 7, 9, 11, 14, 16, 17 and 18) was used in this study [Abbreviation expanded on Page 3 of this Supplementary Information]. This data set was produced with the goal of improving data quality in the northerly lands where the growing seasons are short, using improved calibration procedures unlike its previous counterpart[8,31] (NDVIg).

The NDVI3g data set has a spatial resolution of 8km by 8km per pixel. The maximum NDVI value over a 15-day period is used to represent each 15-day interval to minimize corruption of vegetation signal from atmospheric effects, scan angle effects, cloud contamination and effects of varying solar zenith angle at the time of measurement[32]. This compositing scheme results in two maximum-value NDVI composites per month. The entire available NDVI3g record - July 1981 to December 2011 – was used in this study. Only positive NDVI values that occurred when the surface soils were thawed were used in all the analysis. This assured that the NDVI values corresponded to the period when the vegetation was potentially photosynthetically active (Supplementary Information S2.B).

The NDVI is a radiometric measure of the amount of photosynthetically active radiation (~ 400 to 700 nm) absorbed by chlorophyll in the green leaves of a vegetation canopy[33] and has proven to be a good surrogate of vegetation photosynthetic activity[3]. However, NDVI changes discussed in this article should not be interpreted in terms of terrestrial carbon exchanges, such as net primary production, net ecosystem exchange, etc.

S1.B. MODIS NDVI Data

The latest version of NDVI data (Collection 5) from the MODIS instrument aboard NASA's Terra satellite was used to evaluate the quality of AVHRR NDVI3g data during the

4

1 overlapping period: February 2000 (start of the MODIS record) to December 2011. Unlike

2 AVHRR, MODIS has on-board calibration and precise orbital maintenance. These features

3 combined with narrow spectral bands, higher radiometric precision, atmospheric

4 correction with physics-based algorithms and multiple re-processing of the MODIS data

5 archive with progressively refined algorithms have resulted in improved research-quality

6 vegetation index products. The method described in Xu et al.[34] was used to select the best-

7 quality MODIS NDVI data.

8 The MODIS NDVI data are of shorter duration (Feb 2000 onwards). Moreover, the

9 Terra MODIS instrument developed an anomaly since 2009 and this has reduced the

10 quality of MODIS NDVI since then[35]. Nevertheless, comparison of NDVI3g to MODIS NDVI

11 was performed (Supplementary Table S10). Results from NDVI3g are also compared to

12 those from an earlier version (NDVIg) in Supplementary Information S3.A.

13 **S1.C. Surface Temperature Data**

14 Near-surface air temperature data over land (5° by 5°) from the Climatic Research

15 Unit (CRU) at the University of East Anglia, UK, for the period 1951 to 2011 were used in

16 this study. CRU provides both anomaly (CRUTEM4) and base period absolute temperature

17 data, which allows evaluation of temperature values in each 5° by 5° grid cell.

18 Two higher-resolution (0.5^o by 0.5^o) temperature data sets were also used in this

19 study. The first is the CRU-TS 3.1 for the period January 1981 to December 2009. The

20 second is the NOAA NCEP CPC data set for the period January 1981 to December 2011. All

21 data sets are publicly available. These data were used in different parts of this study to

22 ensure robust results (Supplementary Information S3.B).

23 **S1.D. Freeze/Thaw Data**

24 Daily records of landscape freeze/thaw data for the period 1st January 1988 to 31st

25 December 2007 were obtained from NSIDC. The data records include daily AM

26 freeze/thaw, PM freeze/thaw and combined freeze/thaw, among other parameters at a

5

1 spatial resolution of 25km by 25km[36]. The combined parameter, which describes daily AM

2 and PM thawed or frozen ground state, both measured independently, was used to

3 estimate dates of spring thaw and autumn freeze as described in Supplementary

4 Information S2.B.

5 **S2. Supplementary Methods and Analysis**

6 **S2.A. Definitions of Temperature and Vegetation Seasonality**

7   The objective is to develop definitions of temperature seasonality, S_T, and

8 seasonality of vegetation photosynthetic activity, S_V. These can be defined concordantly as,

$$S_T(l) = \left[1 \div \overline{T}(l) \right], \qquad \text{Eq. (1)}$$

$$S_V(l) = \left[1 \div \overline{N}(l) \right], \qquad \text{Eq. (2)}$$

9   where l is latitude, $\overline{T}(l)$ is mean annual land surface temperature averaged over longitudes

10 on land surfaces except ice sheets, and $\overline{N}(l)$ is mean annual photosynthetic activity

11 averaged over longitudes of Arctic and/or Boreal vegetation shown in Supplementary Fig.

12 S1. These definitions possess three important properties: (1) concordance, (2) ecological

13 underpinning, namely, vegetation photosynthetic activity in the North depends on the

14 seasonal cycle of temperature and not on the difference between annual maximum and

15 minimum temperatures, and (3) satisfy the principle that seasonality increases with

16 latitude at an annual time scale due to patterns of insolation resulting from sun-earth

17 geometry only, i.e. they are heliocentric definitions of seasonality.

18   The zonally-averaged temperature or vegetation photosynthetic activity in Eqs. (1)

19 and (2) can be modeled as

$$Y(x, t) = \alpha + F(x, t), \qquad \text{Eq. (3)}$$

6

where x is sine or cosine of latitude l, t is time during the year, α is a constant and F is a function that characterizes the variation of temperature or vegetation photosynthetic activity during the course of a year with respect to latitude. The functional form of F is different for temperature and vegetation photosynthetic activity because temperature in Kelvin (K) is never equal to zero, while vegetation photosynthetic activity is equal to zero outside of the Photosynthetically Active Period (PAP) due to frozen soils and/or cold air temperatures (PAP < a year). This has two implications.

First, the period of latitudinal variations of temperature is constant, while it varies in the case of vegetation photosynthetic activity. Thus, temperature seasonality may be defined in terms of latitudinal variations in amplitude only, while seasonality of vegetation photosynthetic activity should be defined in terms of latitudinal variations in both its amplitude (annual maximum vegetation photosynthetic activity because the minimum value is zero) and PAP. For this reason, temperature seasonality is conventionally defined as the annual range, i.e. the maximum minus the minimum. The new definition of temperature seasonality introduced here [Eq. (1)] is consistent with the conventional definition of temperature seasonality at an annual scale (*cf.* next section).

Second, temporal variations of temperature are best modeled as a combination of sine and cosine functions, while temporal variations of vegetation photosynthetic activity are best described by a Gaussian function.

Heliocentric definitions of temperature seasonality do not have to be based on annual-mean zonally-averaged temperatures. It is also possible to define "warm-season" temperature seasonality similarly, $S_T(l) = \left[1 \div \overline{T}_{WS}(l) \right]$, where $\overline{T}_{WS}(l)$ is zonally-averaged May-to-September mean temperature. This definition also satisfies the principle that seasonality increases with increasing latitude at an annual time scale due to sun-earth geometry only. Simple analytical models are presented in the following subsections and their validity is established through comparisons with data and further argumentation.

S2.A.1. Definition of Temperature Seasonality

Only a few studies have focused on evaluating whether changes in the phase and amplitude of the annual cycle of temperature observations are comparable with those from climate model simulations with various forcings using respective grid-point data[2,37–39]. Vegetation photosynthetic activity responds to changes in absolute temperature, above some critical threshold value, during the photosynthetically active period, rather than to either temperature changes relative to the annual mean[39] or the difference between the annual maximum and minimum temperatures. Therefore, the following is focused on modeling the latitudinal variation of the annual cycle of absolute land surface temperatures (ice sheets excluded).

Let $\overline{T}_{max}(l)$ and $\overline{T}_{min}(l)$ denote annual-means of daily maximum and minimum near-surface air temperature averaged over longitudes on land surfaces except the ice sheets. This spatio-temporal averaging minimizes impact of factors other than those related to sun-earth geometry on temperature seasonality. $T_{min}(l)$ decreases with latitude l more rapidly than $T_{max}(l)$, such that the range $[T_{max}(l) - T_{min}(l)]$ increases with l (Supplementary Fig. S2a). This range is conventionally defined as temperature seasonality[40,41]. The mean temperature $\overline{T}(l)$ also decreases with l, and therefore, its inverse, $[1 \div \overline{T}(l)]$ increases with l (Supplementary Fig. S2a). This quantity can also be taken as a measure of temperature seasonality. The advantages are two-fold: (a) it is concordant with the definition of vegetation photosynthetic activity (Supplementary Information S2.A.2), (b) it is nearly-equivalent to the conventional definition of temperature seasonality (Supplementary Fig. S2b). This definition also obeys the principle that seasonality increases with increasing latitude at an annual scale (Supplementary Fig. S2). Below, a simple model is outlined to provide a physical foundation for the above reasoning.

The first order approximation of zonally-averaged temperature in a simple two dimensional (latitude and time) energy balance model that includes solar insolation, thermal radiation and horizontal diffusive heat transport is given by

$$T(x,t) = T_0 + (A_{11}\cos 2\pi t + B_{11}\sin 2\pi t)P_1(x) + T_2 P_2(x), \qquad \text{Eq. (4)}$$

1   where x is the sine of latitude l, t is time of the year, and $T(x,t)$ is the average temperature

2   at l[42]. The mean annual temperature is thus determined by coefficients T_0, T_2, and the 2nd

3   Legendre polynomial

4
$$P_2(x) = \tfrac{1}{2}(3x^2 - 1),$$

5   while the amplitude is determined by coefficients A_{11}, B_{11}, and the 1st Legendre polynomial

6    $P_1(x) = x$.

7   If this first order approximation is fit to CRU-TS 3.1 (Supplementary Information

8   S1.C) monthly-mean land surface temperatures from the northern hemisphere, excluding

9   ice-sheets, for the period early-1980s (1982 to 1986), the resulting coefficients are:

10
$$T_0 = 287.3; \; A_{11} = -19.5; \; B_{11} = -6.4; \; T_2 = -30.9.$$

11   The land surface temperatures can be estimated with a Root Mean Square Error (RMSE) of

12    $1.9K$ with these coefficients. The annual-mean land surface temperature $\overline{T}(l)$ (in K) at

13   latitude l in the northern hemisphere can be estimated as

14
$$\overline{T}(l) = T_0 + T_2 P_s(x) = 287.3 + \tfrac{-30.9}{2}(3x^2 - 1) = 302.8 - 46.4\,sin^2 l. \qquad \text{Eq. (5)}$$

15   The amplitude $A(l)$ can be estimated as

$$A(l) = 2(A_{11}^2 + B_{11}^2)^{0.5}\,P_1(x) = 41x = 41\sin l. \qquad \text{Eq. (6)}$$

16   The amplitude $A(l)$ represents the conventional definition of temperature seasonality. The

17   inverse of the annual-mean temperature, $1/\overline{T}(l)$, represents the new definition introduced

18   in this article. The two seasonality measures are monotonically, but non-linearly, related

19   and both increase with latitude, as expected,

$$1/[\overline{T}(l)] = 1/[(302.8 - 0.03A^2(l)]. \qquad \text{Eq. (7)}$$

9

1   This is graphically demonstrated in Supplementary Fig. S2b.

2   The above formulation demonstrates the similarity between the conventional

3   definition of temperature seasonality, $A(l)$, and the new definition, $1/\overline{T}(l)$. This article is,

4   however, focused on large zonal bands (Arctic and Boreal regions) that span a range of

5   latitudes (Supplementary Fig. S1). Therefore, it is important to establish a similar

6   equivalency for large zonal bands. For example, if the zonally-averaged temperature

7   between latitude x and 90°N is of interest (Supplementary Fig. S3a), the requisite

8   integration is

$$\overline{T}_x = \int_{x}^{90} dl\, \overline{T}(l)\, wt(l), \qquad\qquad \text{Eq. (8)}$$

9   where $wt(l)$ is the weight determined by the fraction of land area at latitude l calculated

10   from the vegetation map (Supplementary Fig. S1). The weights must be defined in such a

11   way that they sum to unity. Similarly, if the zonally-averaged temperature between latitude

12   45º and x is of interest, where $x > 45$º (e.g. Supplementary Fig. S3b), the requisite

13   integration is

$$\overline{T}_x = \int_{45}^{x} dl\, \overline{T}(l)\, wt(l), \qquad\qquad \text{Eq. (9)}$$

14   and the weights $wt(l)$ should be defined accordingly. As these weights depend on the

15   vegetation map, there is no analytical solution to Eqs. (8) and (9). Numerical integration,

16   however, demonstrates a good correspondence between the conventional and new

17   definition of temperature seasonality even for large zonal belts (Supplementary Fig. S3c).

18   The upper and lower boundaries of the Arctic and Boreal regions vary longitudinally

19   and latitudinally (Supplementary Fig. S1). Therefore, their seasonality variations can be

20   expressed in terms of equivalent variations over zones with boundary latitudes, L_1^oN and

21   L_2^oN, where L_2^oN $> L_1^o$N, in two ways. First, by treating L_2^oN as a constant and L_1^oN as a

22   variable, such that increasing L_1^oN produces a seasonality increment and *vice versa*. Second,

10

by treating L_1^oN as a constant and L_2^oN as a variable, such that decreasing L_2^oN produces a seasonality decrement and *vice versa* (e.g. Supplementary Figs. S3a and S3b). This gives two ways of obtaining the full range of seasonality variation with respect to latitude (Fig. 3d). This is necessary because it is not known *a priori* the value of Arctic and Boreal temperature (and vegetation) seasonality and how these will change over time. For example, if only Eq. (8) is used to derive the range of seasonality for the early-1980s by varying the lower latitudinal boundary x, it is possible that the Boreal region seasonality during the late-2000s might be outside this range. Thus, it is important to use both Eqs. (8) and (9) to obtain the full range of seasonality variations (Fig. 4a and Supplementary Information S2.D).

S2.A.2. Definition of Seasonality of Vegetation Photosynthetic activity

Vegetation photosynthetic activity is represented by a well proven surrogate, the satellite data-based Normalized Difference Vegetation Index (Supplementary Information S1.A). The NDVI exhibits positive values during winter from evergreen vegetation (Supplementary Fig. S4a), although vegetation photosynthetic activity is effectively zero due to frozen soils and/or cold air temperatures. Therefore, only NDVI values during the Photosynthetically Active Period (PAP) are indicative of vegetation photosynthetic activity. Thus, the definition of seasonality of vegetation photosynthetic activity (vegetation seasonality, hereafter) must account for variations in both the amplitude and PAP, as discussed earlier. The amplitude is simply the annual maximum NDVI value. The PAP is defined as the period when the ground is thawed and is determined using satellite-based passive microwave brightness temperature data (Supplementary Information S2.B). Below, a simple model for vegetation seasonality is derived. It satisfies the requisite principle that (vegetation) seasonality increases with increasing latitude.

Zonally-averaged NDVI data over the Arctic and Boreal regions can be approximated using a combination of the Gaussian function in the time domain and power function in the latitude domain, i.e.

$$N(x,t) = \beta_1 + \beta_2 x^{\beta_3} \exp\left[\frac{-(2\pi t - \beta_4)^2}{2\beta_5^2 x^{\beta_6}}\right] + \beta_7 x^{\beta_8}, \qquad \text{Eq. (10)}$$

1   where x is the cosine of latitude, t is time of the year normalized by 2π, and $N(x,t)$ is the

2   zonally-averaged NDVI mentioned above. This model fits all NDVI profiles between 50ᵒN

3   and 75ᵒN, at 1ᵒ latitude interval, quite well (RMSE = 0.04NDVI) with the following retrieved

4   coefficients:

$$\beta_1 = -0.16; \; \beta_2 = 0.61; \; \beta_3 = -0.05; \; \beta_4 = 3.59;$$

5                               $\beta_5 = 1.55; \; \beta_6 = 1.45; \; \beta_7 = 0.75; \; \beta_8 = 1.46.$

6   The Full Width at Sixth of Maximum (FWSM) was found, through iteration, to

7   correspond to the case of minimal standard deviation, at each 1ᵒ zonal band, for the

8   differences between model-predicted and satellite-based estimates of freeze/thaw dates.

9   Therefore, the duration of PAP as a function of x can be written as

$$PAP(x) = 2\sqrt{2\ln 6}\,\beta_5 x^{\frac{\beta_6}{2}} \cdot \frac{365}{2\pi} = 339 x^{0.72}. \qquad \text{Eq. (11)}$$

10   Thus, $N(x,t)$ averaged over the PAP can be estimated as

11    $\overline{N}(x) = \frac{\beta_2}{2}\sqrt{\frac{\pi}{\ln 6}} x^{\beta_3} \, \text{erf}\left(\sqrt{2\ln 6}\,\beta_5 x^{\frac{\beta_6}{2}}\right) + \left(\beta_1 + \beta_7 x^{\beta_8}\right)$

$$= 0.41 x^{-0.05}\,\text{erf}(2.93 x^{0.72}) + (0.75 x^{1.46} - 0.16) \approx$$

12                         $0.41\,\text{erf}(2.93 x^{0.72}) + 0.75 x^{1.46} - 0.16,$ Eq. (12)

13   where erf($\cdot$) is the error correction function, which is a monotonically increasing function.

14   Note that x^{β_3} has very small variations, which can be ignored. The annual maximum NDVI

15   can also be estimated,

$$NDVIMAX(x) = \beta_2 x^{\beta_3} + \left(\beta_1 + \beta_7 x^{\beta_8}\right) \approx 0.45 + 0.75 x^{1.46}. \qquad \text{Eq. (13)}$$

Each of the three quantities – PAP, NDVI averaged over the PAP, and annual maximum NDVI – is a monotonically increasing function of the cosine of latitude, x, i.e. all three quantities monotonically decrease with latitude [Eqs. (11-13)]. Also, note the PAP-mean NDVI (Eq. 12) includes variations due to PAP in the erf($\cdot$) function and variations due to annual maximum NDVI in the rest of the equation. Therefore, vegetation seasonality, when defined in terms of NDVI, is an explicit function of both PAP duration and annual maximum NDVI, unlike temperature seasonality which depends only on the amplitude, as discussed earlier. It is for this reason that temperature seasonality was defined as the inverse of zonally-averaged annual-mean temperature, $1/\overline{T}(l)$. Vegetation seasonality can be similarly defined as $1/\overline{N}(l)$. The two definitions are now concordant [Eqs. (1) and (2)] and obey the principle that seasonality increases with increasing latitude at an annual time scale. This is also true for large zonal belts with latitudinal boundaries L_1^oN and L_2^oN, where L_2^oN $> L_1^o$N (Supplementary Fig. S4b) as in the case of temperature (Supplementary Fig. S3d).

S2.A.3. Justification and Validity of New Definitions of Seasonality

The new definitions of temperature and vegetation seasonality are motivated and justified by the following considerations. Vegetation photosynthetic activity in the north depends on the integrated temperature value above some critical threshold during the year (e.g. as in the concept of growing degree days), not on the difference between maximum and minimum temperatures (all else being optimal). Therefore, a definition of temperature seasonality that captures both the duration when the temperature is above the critical threshold and the maximum value during this period is needed. This is expressed "most simply" by the inverse of the zonal mean temperature averaged over the photosynthetically active period.

This argumentation is supported by the results in Supplementary Fig. S5. The annual average temperature is more closely related to PAP-mean NDVI than the temperature amplitude (Supplementary Fig. S5c *vs.* Supplementary Fig. S5a) because the former is based on the entire annual cycle of temperature while the latter is based on just

13

1 two values – maximum and minimum temperatures. For the same reason, the new

2 definition of temperature seasonality is more closely related to vegetation seasonality than

3 the conventional definition of temperature seasonality (Supplementary Fig. S5d *vs.*

4 Supplementary Fig. S5b). The wording "more closely related to" is based on the relative

5 root mean square error (RRMSE) of the fit shown in Supplementary Fig. S5.

6   Seasonality variations inferred from analysis based on disparate definitions (e.g.

7 temperature seasonality as annual amplitude and vegetation seasonality as inverse of

8 annual productivity) would be less accurate than those presented in this article because of

9 the poor causal argument underlying temperature amplitude and PAP-mean NDVI which is

10 reflected in the fit of the respective observations (Supplementary Fig. S5a).

11   The new definitions of seasonality are not only based on a meaningful ecological

12 principle, namely, the said connection between integrated temperature above thresholds

13 and vegetation productivity, but also harmonize across two very disparate variables – one

14 physical (temperature) which is never equal to zero (Kelvin) and one biological (vegetation

15 photosynthetic activity) which is equal to zero (carbon flux unit) outside the

16 photosynthetically active period, as mentioned earlier.

17   It is these three features: (1) concordant definitions, (2) ecological underpinning,

18 and (3) heliocentric constraint, that permit inferences regarding seasonality variations in

19 temperature and vegetation during the past 30 years (from measurements; Figs. 4a and 4b)

20 and projections of temperature seasonality variations during the next 100 years (from a

21 suite of coupled climate models (Fig. 4c and Supplementary Table S6).

22   The validity of the new seasonality definition is tested in Supplementary Fig. S6. The

23 temperature profile (i.e. variation during the course of a year) of the Arctic during the

24 reference period (1951 to 1980) corresponded to the temperature profile of all land areas

25 (excluding ice sheets) north of 65°N. Using the new definition introduced here, the

26 temperature seasonality of the Arctic would diminish by an amount equivalent to a

27 southward shift of 18.6° in latitude based on a simulation by a coupled climate model

28 (CCSM4) by the decade 2091 to 2099 (Fig. 4c; Supplementary Table S6). That is, the

14

1 temperature profile of the Arctic in the decade 2091 to 2099 would resemble the

2 temperature profile of all land areas (excluding ice sheets) north of 46.4°N during the

3 reference period. Using an alternate method based on least squares[66], it was found that the

4 temperature profile of the Arctic in the decade 2091 to 2099 corresponds "closest" to the

5 temperature profile of all land areas (excluding ice sheets) north of 46.5°N during the

6 reference period – by "closest" it is meant that the sum of squares of the differences

7 between the two temperature profiles is at a minimum. That is, the sum of squares of the

8 differences between the temperature profile of the Arctic in the decade 2091 to 2099 and

9 the temperature profile north of every other latitude value during the reference period is

10 greater than at north of 46.5°N. This test therefore confirms that the new definition of

11 seasonality accurately captured the entire annual cycle of temperature at the zonal scale.

12

13 **S2.B. Estimating Photosynthetically Active Period (PAP)**

14 The period between the dates of spring thaw and autumn freeze has been reported

15 to be representative of the Photosynthetically Active Period[36,43]. Therefore, the combined

16 parameter in the daily ground-state freeze/thaw data set (specifically, AM and PM thawed

17 ground-state) was used to estimate, for each pixel (p) and year (y), spring thaw date,

18 $[t_1(p, y)]$, as the date corresponding to the 8th day of the first 15 day period in a year,

19 starting from January, when 12 out of 15 days the ground is thawed (AM and PM thawed).

20 Similarly, the end date of landscape thaw in the autumn, $[t_2(p, y)]$, was estimated as the

21 date corresponding to the 8th day of the last 15 day period in a year when 12 out of 15 days

22 the ground is thawed (AM and PM thawed). The resulting dates $t_1(p, y)$ and $t_2(p, y)$ were

23 averaged over the 20-year period of the record (1988 to 2007) because the freeze/thaw

24 data series is shorter than the NDVI data series (1981 to 2011). This will introduce an error

25 because a tendency for lengthening ground non-frozen state has been reported[36,44].

26 However, this error is small because the NDVI values about t_1 and t_2 are low and contribute

27 little to the PAP-mean NDVI.

28

15

1 **S2.C. Statistical Methods**

2 **S2.C.1. Models For Trend Analysis**

3   Four models were used to evaluate areal extents of statistically significant ($p<0.05$
4 and 0.1) changes in PAP-mean NDVI and May-to-September average temperature and
5 corresponding trend magnitudes (Figs. 2a, 3a, 3b, Supplementary Figs. S7, S8 and S9;
6 Supplementary Tables S2, S3 and S4). Models 1, 2 and 4 were used in previous
7 studies[8,10,45,46]. Model 3, introduced in the present study, and Model 4 are robust statistical
8 models – results from these two models are therefore mostly quoted in the manuscript.
9 Below, PAP-mean NDVI is used to illustrate description of the models. The error terms ε in
10 all models are assumed to be independent and identically distributed random variables
11 sampled from a Normal distribution with zero mean and constant variance.

12 **Model 1**: The Simple Linear Trend (SLT) model used in Bhatt et al.[8] is represented by

$$y_t = \alpha + \beta t + \varepsilon_t, \qquad\qquad \text{Eq. (14)}$$

13 where y_t is PAP-mean NDVI of a pixel at time (year) t, α and β are coefficients and ε_t is
14 random error. Statistical significance of the deterministic trend β was tested using the t-
15 distribution. The trend significance will be overstated if the time series is non-stationary[47]
16 or ε_t exhibit serial correlation[48].

17 **Model 2**: This represents one of the statistical models used in previous studies[45,46] with
18 corrections for errors identified in their code and personal communications. This model is
19 not ideally suited for handling non-stationary time series (see Model 4 description).

20 *Step-One*: Auto-Regressive process AR(1) with a constant drift and a deterministic trend
21 term βt, augmented with p lags to account for autocorrelation in the residuals ε_t, also
22 known as the augmented Dickey-Fuller (ADF) test,

16

$$\Delta y_t = \alpha + \beta t + (\gamma - 1)y_{t-1} + \sum_{i=1}^{p} \varphi_i \Delta y_{t-i} + \varepsilon_t, \qquad \text{Eq. (15)}$$

1   where Δy_t is the first-order differenced time series of PAP-mean NDVI, $(y_t - y_{t-1})$, α, β, γ

2   and φ_i are coefficients, Δy_{t-i} is the first-order differenced time series at lag i, and ε_t is

3   random error. The maximum number of lags p was set equal to 4 to be consistent[45,46].

4   Orders from zero to four were considered, where order zero is Eq. (15) without the

5   summation term $\sum_{i=1}^{p} \varphi_i \Delta y_{t-i}$, such that the resulting equation represents an AR(1)

6   process,

$$y_t = \alpha + \beta t + \gamma y_{t-1} + \varepsilon_t, \qquad \text{Eq. (16)}$$

7   i.e.

$$\Delta y_t = \alpha + \beta t + (\gamma - 1)y_{t-1} + \varepsilon_t. \qquad \text{Eq. (17)}$$

8   The accepted model was the one that minimized information loss based on the

9   Akaike Information Criterion[49] (AIC) amongst the set of five fitted models, [AR(1) through

10   AR(5)]. To assure that autocorrelation was successfully removed in the residuals of the

11   accepted model, the Ljung and Box portmanteau test was conducted,

$$Q = N(N + 2) \sum_{k=1}^{M} \left(\frac{\rho(k)^2}{(N - k)} \right), \qquad \text{Eq. (18)}$$

12   where N is the sample size, M is the number of autocorrelation lags, and $\rho(k)$ is the sample

13   autocorrelation at lag k[50]. As suggested in Box et al.[51], M was set equal to 20; which

14   accounts for sample size differences between the previous[45,46] and the current study.

15   Autocorrelation was considered successfully removed if the fitted-model could not be

16   rejected according to a preset threshold ($p<0.1$).

17   Stationarity was assessed on the coefficient $(\gamma - 1)$ using the ADF statistic

18   ($p<0.05$)[52]. If the series was stationary, $(|\gamma| < 1)$, i.e. there is no unit root, the significance

17

of β was tested using the t-distribution to identify whether a statistically significant deterministic trend existed. If yes, the magnitude of the trend was estimated using the simple linear trend model [Eq. (14)] to ensure that the long-term deterministic trend estimation was not biased by the autoregressive terms[53], unlike Goetz et al.[45] but not Bunn and Goetz[46], where both significance assessment and trend were inferred from β of the best lag model based on AIC.

Step-Two: If the fitted-model in step-one was non-stationary, $(\gamma = 1)$, i.e. there is a unit root, the deterministic trend term βt was dropped, and the first-order differenced time series was fitted to the AR process of first-order differences with a drift,

$$\Delta y_t = \alpha + \sum_{i=1}^{p} \varphi_i \Delta y_{t-i} + \varepsilon_t.$$ Eq. (19)

Orders from zero to four were considered, where order zero corresponds to omitting the summation term $\sum_{i=1}^{p} \varphi_i \Delta y_{t-i}$. The accepted model was one that minimized information loss based on AIC amongst the set of five fitted-models. The residuals were tested using the Ljung and Box portmanteau test [Eq. (18)] to ensure that autocorrelation was successfully removed. If yes, α of the accepted model was tested for significance using the t-distribution, while the actual magnitude of the drift was estimated using lag order zero, i.e.

$$\Delta y_t = \alpha + \varepsilon_t,$$ Eq (20)

which ensured that the overall drift value was not biased by the autoregressive terms[53], unlike the previous[45,46] where both significance assessment and drift were inferred from α of the best lag model based on AIC.

In the code provided by the authors[45,46], the term $(\gamma - 1)y_{t-1}$ was included, i.e. instead of Eq. (19), the following model was used[45,46],

18

$$\Delta y_t = \alpha + (\gamma - 1)y_{t-1} + \sum_{i=1}^{p} \varphi_i \Delta y_{t-i} + \varepsilon_t. \qquad \text{Eq. (21)}$$

1 Thus, an additional check with the ADF test for existence of a unit root is needed before

2 testing the significance of α because Eq. (21) represents an alternate model for the same

3 time series and the fitted-model should be checked for stationarity, which the previous[45,46]

4 did not do. To avoid this, Eq. (19) was used in the present study, instead of Eq. (21).

5 **Model 3**: Results from this model are presented in the manuscript because the model

6 captures lingering effects of prior observations and prior random errors in the NDVI data

7 series which have been assembled with data from several different sensors over a period of

8 over 30-years[31,54–56].

9   The model is the standard Box-Jenkins Auto-Regressive Integrated Moving Average

10 [ARIMA(p,d,q)], where p represents the number of Auto-Regressive (AR) terms, q

11 represents the number of Moving Average (MA) terms and d is the number of nonseasonal

12 differences required to make the time series stationary[51]. The AR represents the lasting

13 effects of prior observations and MA represents lasting effects of prior random errors. Note

14 that the second-step of Model 2 [Eq. (19)] is an ARIMA(p,1,0) model with drift. The ARIMA

15 models are useful when the data series are suspected to be non-stationary, in which case

16 differencing will make the series stationary. For example, the PAP-mean NDVI, y, for each

17 pixel in year t was modeled as

$$\Delta y_t = \alpha + \varepsilon_t + \sum_{i=1}^{p} \varphi_i \Delta y_{t-i} + \sum_{i=1}^{q} \theta_i \varepsilon_{t-i}, \qquad \text{Eq. (22)}$$

18 where Δy_t represents the first-order differenced time series, α, φ_i and θ_i are coeffcients,

19 Δy_{t-i} is the first-order differenced time series at lag i, and ε_t is random error. Lag orders

20 p and q from 1 to 2 were considered because the goal is to find the most parsimonious

21 model that adequately describes the data. Further, in order to not over-difference the time

22 series, only first-order differences were used, which is equivalent to assuming that the time

19

1   series has a constant average trend. The accepted model was that which minimized AIC.

2   The residuals were tested using the Ljung and Box portmanteau test [Eq. (18)]. If this test

3   was successful, the drift α was tested for significance using the t-distribution.

4   **Model 4**: Statistical models that assume stationary errors (e.g. Model 1) will result in

5   spurious significance if the time series has a unit root. On the other hand, statistical

6   methods that deal with non-stationary errors often suffer from low power (e.g. Model 2),

7   and are further affected by the parameters chosen (e.g. different autocorrelation lags in

8   Model 2). Therefore, Vogelsang proposed a robust general model for trend estimation with

9   no requirement of *apriori* knowledge as to whether the time series is stationary or non-

10   stationary, and which also avoids estimation of autocorrelation parameters[57,58]. Results

11   from this model are presented in the manuscript for these reasons and as an alternate to

12   Model 3 (e.g. Fig. 3a and 3b). This model has also been used in the previous studies[10,45,46].

13   By forming partial sums of the time series, the simple linear trend [Eq. (14)] can be

14   transformed to

$$z_t = \alpha t + \beta \left[\frac{1}{2}(t^2 + t) \right] + S_t, \qquad \text{Eq. (23)}$$

15   where $z_t = \sum_{j=1}^{t} y_j$ and $S_t = \sum_{j=1}^{t} \varepsilon_j$. The OLS estimate of β in this equation is the linear

16   trend estimation. β is then evaluated for statistical significance using the $t - PS_T$ test. It is

17   robust, as the test is designed to have power when the error is stationary, and remains

18   robust if there is high autocorrelation or a unit root in the errors. In addition, it also has

19   high power for finite sample-size tests. Obviously, it avoids parameter selections such as

20   autocorrelation lag lengths as in the case of certain models for dealing with non-stationary

21   errors (e.g. Model 2).

22   **S2.C.2. Regression Analysis**

23   A way to avoid spurious association between two variables in a regression

24   analysis[47] is to include a deterministic variable in the equation. This has the effect of

detrending the original time series. Thus, the following regression model was used in current study,

$$Y = \beta_0 + \beta_1 X + \beta_2 \text{ time} + \varepsilon, \qquad \text{Eq. (24)}$$

where Y is the dependent variable, time is the deterministic variable, X is the independent variable, β_0, β_1 and β_2 are the regression coefficients, and ε is random error. This specification is acceptable only if the dependent variable contains a deterministic trend; if the dependent variable contains a stochastic trend, detrending will introduce errors. Unfortunately, it is difficult to differentiate between deterministic and stochastic trends for short time periods[59,60]. An alternate regression model to reduce the likelihood of a spurious regression was used in the current study,

$$\Delta Y = \beta_0 + \beta_1 \Delta X + \varepsilon. \qquad \text{Eq. (25)}$$

Here ΔY and ΔX are the first differences of X and Y, and β_0, β_1 and ε are as in Eq. (24). These models were used in a similar context in our prior work and the statistical basis for these choices can be found there[9]. These two regression models were used to test the significance of association between anomalies of vegetation and temperature seasonality (insets in Fig. 3c and 3d; numerical values in Supplementary Table S5) and between PAP-mean NDVI anomalies from AVHRR and MODIS data (Supplementary Table S10).

S2.D. Warm-season Temperature Seasonality Diminishment (Fig. 4a)

Two baselines are required to capture the range of variation in temperature seasonality between 50°N and 75°N at the annual scale. These baselines were evaluated using 1982 to 1986 CRUTEM4 temperature data (Supplementary Information S1.C), a period short enough to preclude secular temperature trends but assures smoother profiles.

For the first baseline, let $S(L^o N : 90^o N; 1982:1986)$ denote the early-1980s May-to-September, i.e. warm-season, temperature seasonality over the Arctic and Boreal vegetated

21

1 lands between the latitudes L^oN and 90ºN. It is evaluated as the inverse of the

2 corresponding temperature,

$$S(L^oN: 90^oN; 1982: 1986) = 1 \div < \overline{T} > (L^oN: 90^oN; 1982: 1986), \qquad \text{Eq. (26)}$$

3 where T is temperature, $\overline{T}$ is warm-season average temperature and $< \overline{T} >$ is the spatial

4 average of $\overline{T}$ between latitudes L^oN and 90ºN. This spatial averaging is performed only

5 over the Arctic and Boreal vegetated lands (Supplementary Fig. S1). The seasonality,

6 $S(L^oN: 90^oN; 1982: 1986)$, resulting by varying L^oN between 50ºN to 75ºN is shown in Fig.

7 4a as the blue baseline.

8   For the second baseline, let $S(45^oN: L^oN; 1982: 1986)$ denote the early-1980s May-

9 to-September temperature seasonality over the Arctic and Boreal vegetated lands between

10 45ºN and L^oN, where $L^oN > 45^oN$. The seasonality, $S(45^oN: L^oN; 1982: 1986)$, resulting by

11 varying L^oN between 50ºN to 75ºN is shown in Fig. 4a as the brown baseline.

12   The Arctic and Boreal temperature seasonalities for various time periods in Fig. 4a

13 were evaluated as follows. For example, let $S(A_{WC}; 1982: 1986)$ denote the early-1980s

14 May-to-September temperature seasonality over Arctic vegetated lands exhibiting

15 statistically significant ($p<0.1$) increases or decreases in warm-season temperature. It is

16 evaluated as the inverse of the corresponding temperature,

$$S(A_{WC}; 1982: 1986) = 1 \div < \overline{T} > (A_{WC}; 1982: 1986), \qquad \text{Eq. (27)}$$

18 where T is temperature, $\overline{T}$ is warm-season average temperature and $< \overline{T} >$ is spatially

19 average of $\overline{T}$ over the Arctic vegetated lands exhibiting statistically significant ($p<0.1$)

20 increases or decreases in warm-season temperature (Supplementary Fig. S8c). Locations

21 exhibiting no statistically significant changes are not included because their warm-season

22 temperature has not changed – including them would be equivalent to adding zeros to a

23 summation operation. The resulting seasonality is plotted on the appropriate baseline as an

24 asterisk and the corresponding latitude is shown in Fig. 4a. The same procedure is then

22

1   applied to the Boreal vegetation (filled-circles in Fig. 4a). The evaluation of Arctic and

2   Boreal temperature seasonalities for periods mid-1990s (1995 to 1997) and late-2000s

3   (2006 to 2010) in Fig. 4a was performed similarly.

4   **S2.E. Baselines of Vegetation Seasonality (Fig. 4b)**

5   As in the case of temperature (Fig. 4a), two baselines are required to capture the

6   range of variation in seasonality of vegetation photosynthetic activity between the latitudes

7   50°N and 75°N at the annual scale. These baselines were evaluated using 1982 to 1986

8   AVHRR NDVI data, a period short enough to preclude secular NDVI trends but assures

9   smoother profiles.

10   For the first baseline, let $S(L^oN:90^oN;1982:1986)$ denote the early-1980s

11   seasonality of Arctic and Boreal vegetation photosynthetic activity between the latitudes

12   L^oN and 90°N. It is evaluated as the inverse of the corresponding NDVI, averaged over the

13   PAP, i.e.

$$S(L^oN:90^oN;1982:1986) = 1 \div < \overline{NDVI} > (L^oN:90^oN;1982:1986), \qquad \text{Eq. (28)}$$

14   where

$$< \overline{NDVI} > (L^oN:90^oN;1982:1986) =$$

$$\frac{1}{(t_2 - t_1)} \int_{t_1}^{t_2} dt < NDVI > (t;L^oN:90^oN;1982:1986). \qquad \text{Eq. (29)}$$

15   The symbols t_1 and t_2 denote the start and end dates of PAP as estimated from

16   ground-state freeze/thaw data (Supplementary Information S2.B). They are defined as

17   when 5% of the Arctic and Boreal vegetated lands between the latitudes L^oN and 90°N are

18   thawed in the spring (t_1) and remain thawed in autumn (t_2).

19   The early-1980s NDVI temporal profile of Arctic and Boreal vegetated lands

20   between the latitudes L^oN and 90°N in Eq. (29) is evaluated as

23

$$< NDVI > (t; L^oN: 90^oN; 1982: 1986) \ =$$

$$(1/5) \sum_{yr=1982}^{yr=1986} \int_{L^oN}^{90^oN} dx \int_{0}^{360} dy \ wt(x,y) NDVI(x,y,t;yr). \qquad \text{Eq. (30)}$$

1 In the above, x is latitude, y is longitude, t is time, yr is year, *wt(x,y)* is a normalized weight,

2 as in Eq. (8), *provided (x,y) pertain to Arctic and Boreal vegetated regions* (Supplementary

3 Fig. S1). Only positive NDVI values were used in order to eliminate corrupted data. The

4 resulting seasonality, $S(L^oN: 90^oN; 1982: 1986)$, by varying the latitude L^oN between 50oN

5 to 75oN is shown in Fig. 4b as the blue baseline.

6   For the second baseline, let $S(45^oN: L^oN; 1982: 1986)$ denote the early-1980s

7 seasonality of Arctic and Boreal vegetation photosynthetic activity between the latitudes

8 45oN and L^oN, where L^oN $> 45^o$N. The rest of the calculations are similar, with one

9 exception,

$$< NDVI > (t; 45^oN: L^oN; 1982: 1986) \ =$$

$$(1/5) \sum_{yr=1982}^{yr=1986} \int_{45^oN}^{L^oN} dx \int_{0}^{360} dy \ wt(x,y) NDVI(x,y,t;yr), \qquad \text{Eq. (31)}$$

10 and a corresponding definition of the weights. The resulting seasonality,

11 $S(45^oN: L^oN; 1982: 1986)$, by varying the latitude L^oN between 50oN to 75oN is shown in

12 Fig. 4b as the brown baseline.

13 **S2.F. Arctic and Boreal Vegetation Seasonality Diminishment (Fig. 4b)**

14   Let $S(A_{GB}; 1982: 1986)$ denote the early-1980s seasonality of vegetation

15 photosynthetic activity of *greening and browning locations* in the Arctic, i.e. those parts in

16 the Arctic (Supplementary Fig. S1a) where the vegetation exhibits a statistically significant

17 (*p*<0.1) change in PAP-mean NDVI (Fig. 2a). It is evaluated as the inverse of early-1980s

18 NDVI of these greening and browning Arctic locations averaged over the PAP, i.e.

24

1
$$S(A_{GB}; 1982{:}1986) = 1 \div < \overline{NDVI} > (A_{GB}; 1982{:}1986), \qquad \text{Eq. (32)}$$

2 where

$$< \overline{NDVI} > (A_{GB}; 1982{:}1986) =$$

$$\frac{1}{(t_2 - t_1)} \int_{t_1}^{t_2} dt < NDVI > (t; A_{GB}; 1982{:}1986). \qquad \text{Eq. (33)}$$

3 The symbols t_1 and t_2 denote the start and end dates of PAP. They are defined as when 5%
4 of the greening and browning locations in the Arctic are thawed in the spring (t_1) and
5 remain thawed in autumn (t_2). The early-1980s NDVI temporal profile of Arctic greening
6 and browning locations in Eq. (33) is evaluated as

$$< NDVI > (t; A_{GB}; 1982{:}1986) =$$

$$(1/5) \sum_{yr=1982}^{yr=1986} \int_{0}^{90N} dx \int_{0}^{360} dy \, wt(x,y) NDVI(x,y,t;yr), (x,y) \in A_{GB}. \quad \text{Eq. (34)}$$

7 In the above, x is latitude, y is longitude, t is time, yr is year, $wt(x,y)$ is a normalized weight,
8 as in Eq. (8), *provided (x,y) belongs to greening and browning locations in the Arctic.*
9 Locations exhibiting no statistically significant changes are not included because their PAP-
10 mean NDVI has not changed – including them would be equivalent to adding zeros to a
11 summation operation. Further, only positive NDVI values were used in order to eliminate
12 corrupted data. The seasonalities for the mid-1990s, $S(A_{GB}; 1995{:}1997)$, and late-2000s,
13 $S(A_{GB}; 2006{:}2010)$, were evaluated similarly. The seasonalities for the Boreal greening and
14 browning locations for the three time periods were evaluated likewise and are shown in
15 Fig. 4b.

16

17

25

S2.G Model Projections of Temperature Seasonality Diminishment (Fig. 4c)

All temperature data in Fig. 4c are from the National Center for Atmospheric Research (NCAR) Community Climate System Model 4 (CCSM4) forced with Representative Concentration Pathway (RCP) 8.5[30] as contribution to the Coupled Model Intercomparison Project 5 (CMIP5[4]). The baseline in Fig. 4c is evaluated as follows. Let $S(L^oN: 90^oN; 1951: 1980)$ denote the baseperiod (1951 to 1980) temperature seasonality of all lands (vegetated or barren but excluding ice sheets) between the latitudes L^oN and 90oN. It is evaluated as the inverse of the corresponding temperature,

$$S(L^oN: 90^oN; 1951: 1980) = 1 \div < \bar{T} > (L^oN: 90^oN; 1951: 1980), \quad \text{Eq. (35)}$$

where T is temperature, $\bar{T}$ is annual average temperature and $< \bar{T} >$ is the spatial average of $\bar{T}$ between latitudes L^oN and 90oN. The seasonality, $S(L^oN: 90^oN; 1951: 1980)$, resulting by varying L^oN between 10oN to 75oN is shown in Fig. 4c as the blue baseline.

The Arctic and Boreal temperature seasonalities for different time periods in Fig. 4c were evaluated as follows. For example, let $S(A; 2091: 2099)$ denote the annual temperature seasonality over the Arctic vegetated lands for the period 2091 to 2099. It is evaluated as the inverse of the corresponding temperature,

$$S(A; 2091: 2099) = 1 \div < \bar{T} > (A; 2091: 2099), \quad \text{Eq. (36)}$$

where T is temperature, $\bar{T}$ is annual average temperature and $< \bar{T} >$ is spatial average of $\bar{T}$ over the Arctic vegetated lands (Supplementary Fig. S1a). The resulting seasonality is plotted on the baseline and the corresponding latitude is shown in Fig. 4c. The evaluation of Arctic and Boreal temperature seasonalities for other time periods was performed similarly. The projected diminishment in temperature seasonality between the baseperiod (1951 to 1980) and the final decade of 21st century (2091 to 2099) is also shown in Fig. 4c.

26

S3. Supplementary Results and Discussion

S3.A. Comparative Analysis

Results from the current study are consistent with previous studies[9,61] and reflect a spatially-fragmented or discontinuous pattern of PAP-mean NDVI changes in the Boreal region of North America, unlike Eurasia (Models 3 and 4 results in Supplementary Fig. S7). Other studies have reported browning of boreal forests, particularly in North America[10,45,46]. A strict comparison of results published in these studies[10,45,46] with results of the current study is not possible because of differences in NDVI data sets, record lengths and methods of analysis. Nevertheless, a comparative analysis along the following lines allows for a resolution of these divergent results.

(1) <u>Differences in spatial extent of NDVIg and NDVI3g</u>. The NDVIg data (earlier version) displays an artificial discontinuity at 72°N because it used SPOT sensor data for intercalibration. The NDVI3g data (latest version and basis of this article) corrects for this anomaly by using SeaWiFS sensor data for intercalibration[8]. Therefore, the comparative analysis here is restricted to vegetated areas (defined below) between 45°N and 70°N.

(2) <u>Differences in quality of NDVIg and NDVI3g</u>. The NDVIg data were developed using southern targets (e.g. the Sahara desert) for stability while NDVI3g data development used higher-latitude targets (e.g. Northern oceans). Together with the above-mentioned inter-sensor calibration tied to the SeaWiFS sensor, NDVI3g has better overall calibration and is better suited to studies of northern ecosystems[8]. Comparisons of NDVI3g data with similar data from a new sensor, Terra MODIS, has consistently shown good agreement[8] (also Supplementary Table S10). The previous studies[10,45,46] used NDVIg data while the current study is based on NDVI3g data. Therefore, this comparative analysis is as much a study of the differences between NDVIg and NDVI3g data sets as differences between previous studies[10,45,46] and the current article.

27

1   (2) <u>Differences in study areas</u>. Vegetated areas in the 45ºN to 70ºN region were divided into

2   three classes using the latest version (Collection 5) of the MODIS lGBP land cover

3   classification map[62,63]: (a) Boreal forests (evergreen needleleaf forests, deciduous

4   needleleaf forests and mixed forests) with woody fraction greater than 30%, (b) Other

5   natural vegetation (broadleaf forests, closed and open shrublands, woody grasslands and

6   grasslands), and (c) Land cover types not included in the analysis (croplands,

7   cropland/natural vegetation mosaics, permanent wetlands, barren or sparsely vegetated,

8   urban and built-up, snow and ice, water, and unclassified). The woody fraction of boreal

9   forests was determined with the latest version (Collection 5) MODIS Vegetation Continuous

10   Fields product which provided woody fraction in pixels of size 250m by 250m[64]. A similar

11   second calculation was performed by defining boreal forests (same land cover types as

12   above) but with woody fraction greater than 40%. The results are discussed separately for

13   two categories of vegetation types:

14   • <u>Boreal Forests</u>, as defined above, with 30% and 40% woody fraction

15   (Supplementary Information S3.A.1)

16   • <u>Northern Vegetation</u>, which includes boreal forests and other natural vegetation

17   (broadleaf forests, closed and open shrublands, woody grasslands and grasslands) –

18   Supplementary Information S3.A.2.

19

20   (3) <u>Differences in statistical methodologies</u>. A robust statistical method, Model 4[58] in

21   Supplementary Information S2.C.1, was used to assess statistical significance at $p<0.1$. This

22   was one of the methods used in the previous studies[10,45,46].

23   (4) <u>Differences in NDVI metric used for assessing statistically significant changes</u>. Different

24   periods of growing season length were used in previous studies[10,45,46]. For comparison

25   sake, the May-to-September average NDVI was used as the metric for statistical analysis

26   here. Only positive NDVI values were used to avoid inclusion of invalid data. The analysis

27   was performed only if 9 out of 10 NDVI values were positive (the NDVIg and NDVI3g data

28   are 15-day composites, i.e. there is one NDVI value per pixel for every 15-days; 2 such

1 values for each month; hence a maximum of 10 valid values for the five-month period, May-

2 to-September).

3 (5) <u>Differences in NDVI record length</u>. The calculations were performed for the period

4 1982 to 2006. To assess the impact of record length, a second set of calculations was

5 performed with NDVI3g for the period 1982 to 2011. The publicly available NDVIg data are

6 for the period 1982 to 2006, although Beck and Goetz[10] used a slightly extended NDVIg

7 record, 1982 to 2008, while the earlier studies[45,46] used NDVIg for the period 1982 to

8 2003.

9 Results from a comparative analysis along the above lines are shown in

10 Supplementary Fig. S10 and tabulated in Supplementary Tables S8 and S9. In the

11 presentation below, statistically significant increase ($p<0.1$) in May-to-September average

12 NDVI is termed "greening" and statistically significant ($p<0.1$) decrease in May-to-

13 September average NDVI is termed "browning."

14 The following conclusions can be drawn: (1) At the circumpolar scale, a small

15 proportion of boreal forests and other natural vegetation is browning (<5% of the

16 respective areas). (2) The greening proportion is greater than the browning proportion in

17 both Eurasia and North America. (3) The browning proportion is greater than the greening

18 proportion only in the boreal forests of North America. (4) These results are independent

19 of the data set versions (NDVIg or NDVI3g), length of data record (1982 to 2006 or 1982 to

20 2011) and definition of boreal forests (>30% or >40% woody fraction).

21 The following caveat is in order: The greening, browning and no-change proportions

22 quoted in the main manuscript are more accurate than those quoted here for three reasons.

23 First, spatially varying photosynthetically active period (PAP) based on freeze/thaw data

24 was used in the main manuscript, while the PAP is fixed as May-to-September period here

25 to allow a methodologically consistent comparison with previous studies. Second, the use

26 of NDVI3g in the main manuscript allows inclusion of vegetated regions north of 70°N

27 while the analysis here is restricted to 70°N to allow a spatially consistent comparison with

28 previous studies. Third, differences in vegetation maps between the main manuscript

1 (Supplementary Fig. S1) and the analysis here (e.g. inclusion of broadleaf forests, as

2 described above in item 2), again to insure methodological consistency with previous

3 studies.

4 **S3.A.1. Boreal Forests**

5 **<u>North America</u>**

6 (1) About 87% of the boreal forests show no statistical significant changes in May-to-

7 September average NDVI (Supplementary Table S8).

8   • This proportion is independent of NDVI data set for the period 1982 to 2006.

9   • This proportion decreases to 82% as the record is extended to 2011 using the

10   NDVI3g data set.

11

12 (2) Of the remaining 13% of boreal forests,

13   • The data sets disagree for the period 1982 to 2006. NDVIg shows 10% browning

14   and 3% greening. NDVI3g shows equal proportions of browning and greening

15   (6%).

16   • The browning proportion increases to 11% and greening proportion increases

17   to 7% as the NDVI3g data record is extended to 2011.

18

19 (3) These results do not change if the boreal forests are re-defined as having more than

20 40% woody fraction (Supplementary Table S9).

21 **<u>Eurasia</u>**

22 (1) The proportion of boreal forest that shows no statistically significant changes differs

23 between NDVIg (81%) and NDVI3g (54%; Supplementary Table S8).

- This is due to a switch from statistically insignificant changes in NDVIg to statistically significant increase (greening) in NDVI3g, predominantly in the boreal forests of the Western half of Eurasia (Supplementary Fig. S10).

(2) Both data sets show a higher proportion of greening than browning (17% vs. 2% in NDVIg; 45% vs. 0.2% in NDVI3g). The greening proportion is much greater in the NDVI3g data set than the NDVIg data set.

(3) The NDVI3g results do not change as the data record is extended to 2011.

(4) The results do not change if the boreal forests are re-defined as having more than 40% woody fraction (Supplementary Table S9).

Circumpolar

(1) About 66 to 83% of boreal forests show no statistically significant changes in May-to-September average NDVI (Supplementary Table S8).

(2) Both data sets show a higher proportion of greening than browning (12% vs. 5% in NDVIg; 32% vs. 2% in NDVI3g). The greening proportion is much greater in the NDVI3g data set than the NDVIg data set.

(3) The NDVI3g results do not change as the data record is extended to 2011 (2% more browning proportion and corresponding reduction in area of statistically insignificant changes).

(4) The results do not change if the boreal forests are re-defined as having more than 40% woody fraction (Supplementary Table S9).

S3.A.2. Northern Vegetation

North America

(1) About 84 to 88% of natural vegetation (boreal forests and other natural vegetation) shows no statistical significant changes in May-to-September average NDVI (Supplementary Table S8).

- This proportion is independent of NDVI data set for the period 1982 to 2006.
- This proportion decreases to 74% as the NDVI3g data record is extended to 2011.

(2) Of the remaining 12 to 16% of the natural vegetation,

- The greening proportion is about 6% in the NDVIg data and 12% in the NDVI3g data for the period 1982 to 2006. The browning proportion is about 6% in the NDVIg data and 4% in the NDVI3g data during the same time period.
- The greening proportion increases to 18% and browning proportion increases to 8% as the NDVI3g data record is extended to 2011.

(3) The results do not change if the boreal forests, ,are re-defined as having more than 40% woody fraction (Supplementary Table S9).

Eurasia

(1) About 65 to 80% of natural vegetation shows no statistically significant changes in May-to-September average NDVI (Supplementary Table S8).

(2) Both data sets show a higher proportion of greening than browning (18% vs. 3% in NDVIg; 34% vs. 0.6% in NDVI3g). The greening proportion is much greater in the NDVI3g data set than the NDVIg data set.

(3) The NDVI3g results do not change as the data record is extended to 2011.

32

(4) The results do not change if the boreal forests, which are part of the natural vegetation, are re-defined as having more than 40% woody fraction (Supplementary Table S9).

Circumpolar

(1) About 72 to 82% of natural vegetation shows no statistically significant changes in May-to-September average NDVI (Supplementary Table S8).

(2) Both data sets show a higher proportion of greening than browning (14% vs. 4% in NDVIg; 26% vs. 2% in NDVI3g).

(3) The NDVI3g results do not change as the data record is extended to 2011 (2% more greening, 2% more browning and a corresponding reduction in area of statistically insignificant changes).

(4) The results do not change if the boreal forests, which are part of the natural vegetation, are re-defined as having more than 40% woody fraction (Supplementary Table S9).

S3.B. Robustness of Results and Conclusions

Three temperature and NDVI data sets were analyzed in this study with several different methods to assure robustness of results and conclusions. These are briefly mentioned below.

The S_T model was developed with the 0.5º by 0.5º CRU TS 3.1 data (Supplementary Fig. S2). The model was tested with 0.5º by 0.5º NOAA NCEP CPC temperature (Fig. 1a). The same NOAA data were used in Figs. 1b, 1c and 3. The 5º by 5º CRUTEM4 temperature data were used in Fig. 4 and also to test the S_T model (Supplementary Fig. S3).

Four statistical models were used to evaluate statistical significance at two levels ($p<0.05$ and 0.1) and corresponding trends of temperature and NDVI based quantities (Figs. 2a, 2b, 3a, 3b, Supplementary Figs. S7, S8 and S9; Supplementary Tables S2, S3 and S4).

33

1   Two different regression models were used to evaluate statistical association

2   between temperature and NDVI-related quantities (insets in Figs. 3c and 3d;

3   Supplementary Table S5). A comparative analysis between the earlier version of NDVI data

4   set (NDVIg) and the current version (NDVI3g, the basis of this article) was performed

5   (Supplementary Information S3.A; Supplementary Fig. S10; Supplementary Tables S8 and

6   S9).

7   Regression analyses (Supplementary Table S10) to evaluate the degree of

8   association in anomalies of PAP-mean NDVI over a 12-year overlapping period between

9   AVHRR and MODIS sensors yielded satisfactory results for regression model 2 (Eq. 25) but

10   not for model 1 (Eq. 24). Regression model 1 suffers from uncertainty regarding whether

11   the dependent variable contains a deterministic or stochastic trend which is difficult to

12   resolve if the time series are short, as is the case here (Supplementary Information S2.C.2).

13   Regression model 2 avoids this ambiguity but implicitly assumes that the first-differenced

14   time series are stationary. In any case, the results in Supplementary Table S10 should be

15   interpreted cautiously in view of the short record length (12 years). Moreover, Terra

16   MODIS NDVI data, used as a benchmark in this analysis, may have been compromised due

17   to an instrumental anomaly since 2009[35]. A comprehensive global scale analysis of MODIS

18   NDVI and AVHRR NDVI3g data similarly reports a cautious interpretation of comparisions

19   between the two data sets[65].

20   A test of the validity of the new definitions of seasonality introduced in this article

21   (Supplementary Information S2.A), using temperature seasonality as an example, is shown

22   in Supplementary Fig. S6. This test also informs that the baseline methodology of

23   evaluating seasonality changes in Fig. 4 is accurate[66].

24   **S3.C. Potential Vegetation Response to Projected Temperature Seasonality Decline**

25   The adaptability of extant plant species and poleward migration of productive

26   southerly plant species in response to large projected declines in temperature seasonality

27   during the 21st century (Supplementary Table S6) are not well understood as they depend

28   on a multitude of factors, processes and feedbacks, probably many of which are presently

34

1 unknown. Changes in temperature, precipitation, permafrost thawing, winter warming

2 events, nutrient availability, snow pack, herbivore population etc. can impact the

3 survivability and reproductive ability of plant species[17,67,68]. For example, there is

4 accumulating evidence of increase in the cover of erect deciduous shrubs in the tundra

5 driven mostly by warming and possibly increased snow depths[11,12,14,23]. Extant plant

6 species can also experience climatic constraints, pests, fires and other

7 disturbances[16,17,18,45,69] that may reduce growth, reproductive success, and hence, the

8 frequency and cover of these species. The changing climatic regime, including winter time

9 warming, could have effects on the movement, persistence and competition within and

10 between plant communities[13,17,70]. Poleward migration of productive southerly plant

11 species in response to projected large declines in temperature seasonality might occur, but

12 modeling (e.g. those based on bioclimatic envelopes) suggesting drastic shifts in the

13 distribution of the species may be overly simplistic[71,72], as it is possible that populations

14 may undergo evolutionary changes enabling species to cope with environmental change[73].

35

Supplementary References and Notes

31. Pinzon, J. E. et al. Revisiting error, precision and uncertainty in NDVI AVHRR data: development of a consistent NDVI3g time series. *Remote Sensing* Submitted (2012).

32. Holben, B. Characteristics of maximum-value composite images from temporal AVHRR data. *International Journal of Remote Sensing* **7**, 1417–1434 (1986).

33. Myneni, R. B., Hall, F. G., Sellers, P. J. & Marshak, A. L. The interpretation of spectral vegetation indexes. *Geoscience and Remote Sensing, IEEE Transactions on* **33**, 481 –486 (1995).

34. Xu, L. *et al.* Widespread decline in greenness of Amazonian vegetation due to the 2010 drought. *Geophysical Research Letters* **38**, (2011).

35. Wang, D. *et al.* Impact of sensor degradation on the MODIS NDVI time series. *Remote Sensing of Environment* **119**, 55–61 (2012).

36. Kim, Y., Kimball, J. S., Zhang, K. & McDonald, K. C. Satellite detection of increasing Northern Hemisphere non-frozen seasons from 1979 to 2008: Implications for regional vegetation growth. *Remote Sensing of Environment* **121**, 472–487 (2012).

37. Wallace, C. J. & Osborn, T. J. Recent and future modulation of the annual cycle. *Clim Res* **22**, 1–11 (2002).

38. Thomson, D. J. The Seasons, Global Temperature, and Precession. *Science* **268**, 59–68 (1995).

39. Stine, A. R., Huybers, P. & Fung, I. Y. Changes in the phase of the annual cycle of surface temperature. *Nature* **457**, 435–440 (2009).

40. Andreasson, F. P. & Schmitz, B. Temperature seasonality in the early middle Eocene North Atlantic region: Evidence from stable isotope profiles of marine gastropod shells. *Geological Society of America Bulletin* **112**, 628–640 (2000).

41. Patterson, W. P., Dietrich, K. A., Holmden, C. & Andrews, J. T. Two millennia of North Atlantic seasonality and implications for Norse colonies. *PNAS* (2010).doi:10.1073/pnas.0902522107

42. North, G. R. & Coakley, J. A. Differences between Seasonal and Mean Annual Energy Balance Model Calculations of Climate and Climate Sensitivity. *Journal of the Atmospheric Sciences* **36**, 1189–1204 (1979).

36

43. McDonald, K. C., Kimball, J. S., Njoku, E., Zimmermann, R. & Zhao, M. Variability in Springtime Thaw in the Terrestrial High Latitudes: Monitoring a Major Control on the Biospheric Assimilation of Atmospheric CO2 with Spaceborne Microwave Remote Sensing. *Earth Interactions* **8**, 1–23 (2004).

44. Zhang, K., Kimball, J. S., Kim, Y. & McDonald, K. C. Changing freeze-thaw seasons in northern high latitudes and associated influences on evapotranspiration. *Hydrological Processes* **25**, 4142–4151 (2011).

45. Goetz, S. J., Bunn, A. G., Fiske, G. J. & Houghton, R. A. Satellite-observed photosynthetic trends across boreal North America associated with climate and fire disturbance. *PNAS* **102**, 13521–13525 (2005).

46. Bunn, A. G. & Goetz, S. J. Trends in Satellite-Observed Circumpolar Photosynthetic Activity from 1982 to 2003: The Influence of Seasonality, Cover Type, and Vegetation Density. *Earth Interactions* **10**, 1–19 (2006).

47. Granger, C. W. J. & Newbold, P. Spurious regressions in econometrics. *Journal of Econometrics* **2**, 111–120 (1974).

48. Cochrane, D. & Orcutt, G. H. Application of Least Squares Regression to Relationships Containing Auto- Correlated Error Terms. *Journal of the American Statistical Association* **44**, 32–61 (1949).

49. Akaike, H. A new look at the statistical model identification. *IEEE Transactions on Automatic Control* **19**, 716 – 723 (1974).

50. Ljung, G. M. & Box, G. E. P. On a measure of lack of fit in time series models. *Biometrika* **65**, 297–303 (1978).

51. Box, G. E. P., Jenkins, G. M. & Reinsel, G. C. *Time series analysis: forecasting and control*. (Prentice Hall: 1994).

52. Dickey, D. A. & Fuller, W. A. Distribution of the Estimators for Autoregressive Time Series With a Unit Root. *Journal of the American Statistical Association* **74**, 427–431 (1979).

53. Mathworks Econometrics Toolbox User's Guide (R2012a). (2012).at <http://www.mathworks.com/help/pdf_doc/econ/econ.pdf>

54. Tucker, C. J. *et al.* An extended AVHRR 8-km NDVI dataset compatible with MODIS and SPOT vegetation NDVI data. *International Journal of Remote Sensing* **26**, 4485–4498 (2005).

55. Pinzon, J. E., Brown, M. E. & Tucker, C. J. EMD correction of orbital drift artifacts in satellite data stream. *Hilbert-Huang Transform And Its Applications* **5**, 167–186 (2005).

56. Brown, M. E., Pinzon, J. E., Didan, K., Morisette, J. T. & Tucker, C. J. Evaluation of the consistency of long-term NDVI time series derived from AVHRR,SPOT-vegetation, SeaWiFS, MODIS, and Landsat ETM+ sensors. *IEEE Transactions on Geoscience and Remote Sensing* **44**, 1787 –1793 (2006).

57. Fomby, T. B. & Vogelsang, T. J. The Application of Size-Robust Trend Statistics to Global-Warming Temperature Series. *Journal of Climate* **15**, 117–123 (2002).

58. Vogelsang, T. Trend Function Hypothesis Testing in the Presence of Serial Correlation. *Econometrica* **66**, 123–148 (1998).

59. Nelson, C. R. & Plosser, C. R. Trends and random walks in macroeconmic time series: Some evidence and implications. *Journal of Monetary Economics* **10**, 139–162 (1982).

60. Enders, W. *Applied econometric time series.* (Wiley: 1995).

61. Bogaert, J. Evidence for a persistent and extensive greening trend in Eurasia inferred from satellite vegetation index data. *Journal of Geophysical Research* **107**, (2002).

62. Friedl, M. A. *et al.* MODIS Collection 5 global land cover: Algorithm refinements and characterization of new datasets. *Remote Sensing of Environment* **114**, 168–182 (2010).

63. Friedl, M. . *et al.* Global land cover mapping from MODIS: algorithms and early results. *Remote Sensing of Environment* **83**, 287–302 (2002).

64. Townshend, J. User Guide for the MODIS Vegetation Continuous Fields product Collection 5 version 1. (2011).at https://lpdaac.usgs.gov/sites/default/files/public/modis/docs/VCF_C5_UserGuide_Dec2011.pdf

65. Fensholt, R. & Proud, S. R. Evaluation of Earth Observation based global long term vegetation trends – Comparing GIMMS and MODIS global NDVI time series. *Remote Sensing of Environment* **119**, 131–147 (2012).

66. Let L^oN be the latitude of the southern boundary of a zone that satisfies the condition, $\min\left[\sum_t | T_A(t;D) - T_{>L^oN}(t;B)|^2\right]$, where t is days $\leq$ a year, $T_A(t;D)$ is the temperature profile of the Arctic for a certain decade D between 1981 and 2099 and $T_{>L^oN}(t;B)$ is the temperature profile of lands $>L^oN$, vegetated or barren but not ice sheets, during the base period B (1951 to 1980). This latitude L^oN (Supplementary Fig. S6) matches the latitude inferred using the baseline methodology (corresponding CCSM4 entries in Supplementary Table S6).

67. Walther, G. *et al.* Ecological responses to recent climate change. *Nature* **416**, 389-395 (2002).

68. Olofsson, J. *et al.* Herbivores inhibit climate-driven shrub expansion on the tundra. *Global Change Biology* **15**, 2681–2693 (2009).

69. Hofgaard, A. *et al.* Role of disturbed vegetation in mapping the boreal zone in northern Eurasia. *Appled Vegetation Science* **13**, 460–472 (2010).

70. Woodall, C. W. *et al.* An indicator of tree migration in forests of the eastern United States. *Forest Ecology and Management* **257**, 1434–1444 (2009).

71. Williams, M., Eugster, W., Rastetter, E. B., McFadden, J. P. & Chapin, F. S. The controls on net ecosystem productivity along an Arctic transect. *Global Change Biology,* **6**, 116–126 (2000).

72. Moser, B., Fridley, J. D., Askew, A. P. & Grime, J. P. Simulated migration in a long-term climate change experiment: invasions impeded by dispersal limitation, not biotic resistance. *Journal of Ecology* **99**, 1229–1236 (2011).

73. Morin, X., Viner, D. & Chuine, I. Tree species range shifts at a continental scale: a new predictive insights from a process-based model. *Journal of Ecology* **96**, 784–794 (2008).

74. Walker, D. A. *et al.* The Circumpolar Arctic vegetation map. *Journal of Vegetation Science* **16**, 267–282 (2005).

Vegetation Map

| 1 | 2 | 3 | 4 | 5 | 6 | 7 | 8 | 9 | 10 | 11 | 12 | 13 | 14 |
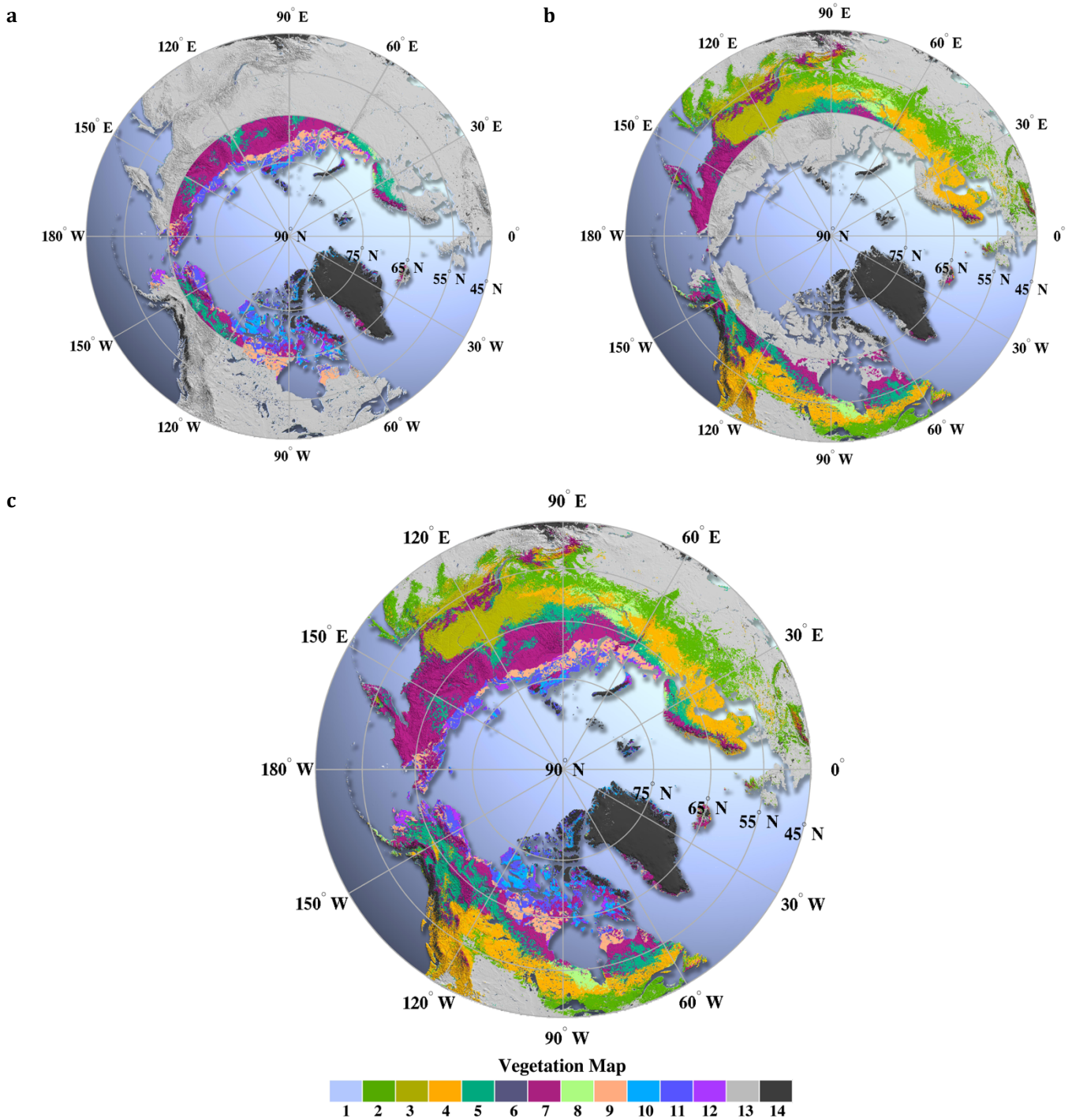
Supplementary Figure S1 | Vegetation map of the Arctic-Boreal region compiled from the Circumpolar Arctic Vegetation Map[74] (CAVM) and the latest version of the MODIS IGBP Land Cover Map[62]. a, Arctic (8.16 million km²) defined as the vegetated area north of 65ºN, excluding crops and forests, but including the tundra south of 65ºN. **b**, Boreal region (17.86 million km²)

defined as the vegetated area between 45°N and 65°N, excluding crops, tundra, broadleaf forests, but including needleleaf forests north of 65°N. Grasslands south of the mixed forests are excluded as these are not conventionally considered as Boreal vegetation. **c**, Combined vegetation map of the Arctic and Boreal regions. The 14 different classes are described in Supplementary Table S1. This vegetation map is based on CAVM and infilling with merged MODIS IGBP Land Cover Map classes where CAVM ended. These Arctic and Boreal definitions are a compromise between ecological and climatological conventions. The vegetation labels are less critical as they include all natural (non-cultivated) vegetation types within these two regions and no vegetation-class dependent analysis was performed in this study.

a

b
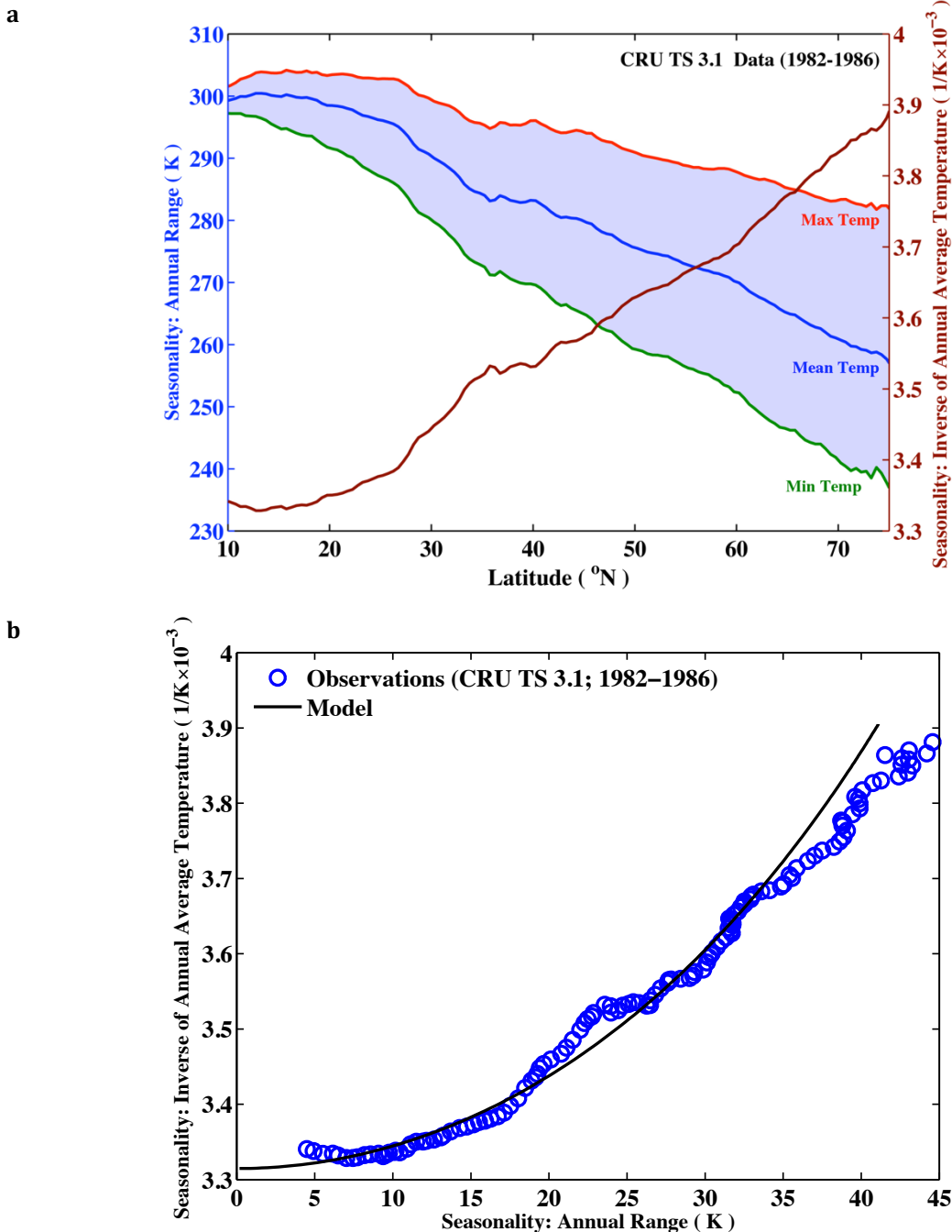
Supplementary Figure S2 | Model testing of land surface temperature seasonality at the latitudinal scale. a, Latitudinal variation of annual-mean maximum, minimum, average and inverse of average land surface temperature (excluding ice sheets). The difference between the maximum and minimum temperature, the annual range shown as the shaded area, is the conventional definition of temperature seasonality. **b**, Temperature seasonality defined as $[1 \div \overline{T}_{yr}(l)]$, where $\overline{T}_{yr}(l)$ is the zonally-averaged annual-mean temperature at latitude l and modeled following North and Coakley[42]. The model predictions are compared to the conventional

3

definition of seasonality (the annual range). The temperature data used in this analysis is the 0.5° by 0.5° CRU TS 3.1 averaged over the years 1982 to 1986. Details in Supplementary Information S2.A.1.

4
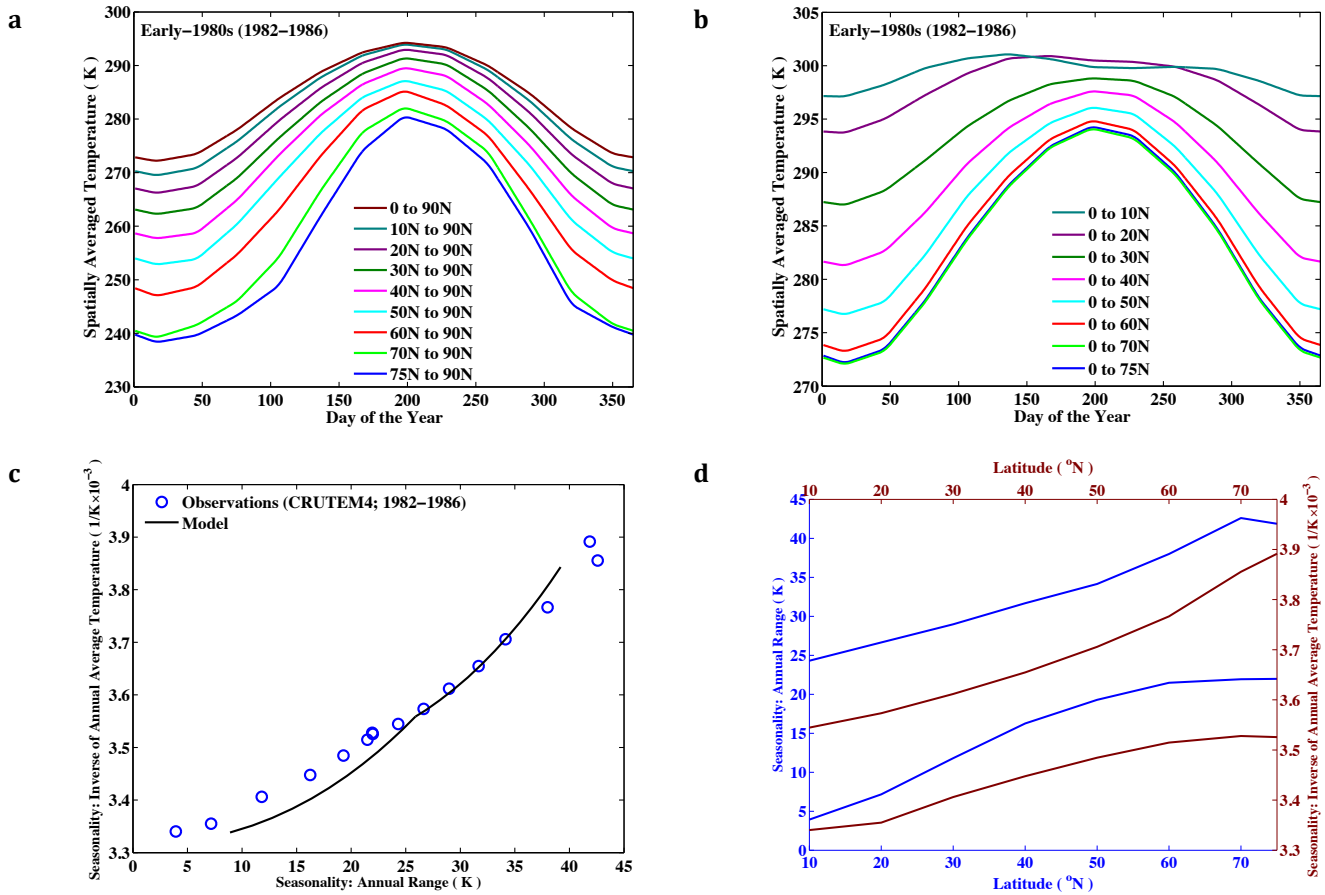
Supplementary Figure S3 | Model testing of land surface temperature seasonality at the zonal scale. a, Annual course of temperature (CRUTEM4) for different zones bounded by latitudes L_1^oN and L_2^oN, where L_2^oN > L_1^oN, holding L_2^oN constant and varying L_1^oN to produce a range of seasonalities. **b**, Same as **a** but holding L_1^oN constant and varying L_2^oN to produce a different range of seasonalities lower than in **a**. **c**, Temperature seasonality defined as [1 ÷ $\overline{T}_{yr}(l)$], where $\overline{T}_{yr}(l)$ is zonally-averaged annual-mean temperature at latitude l and modeled following North and Coakley[42]. This model was integrated across latitudes following Eqs. (8) and (9) and compared to the conventional definition of seasonality (the annual range) evaluated from CRUTEM4 data shown in **a** and **b**, respectively. **d**, The new and conventional definitions at the zonal scale obey the principle that seasonality increases with latitude due to sun-earth geometry only. At each latitude, e.g. 40°N, there are two values of seasonality, for each definition of seasonality – the first corresponds to the zone 40°N to 90°N and the second to 0°N to 40°N. The methodology on how these "baselines" are calculated is described in Supplementary Information S2.D.

a
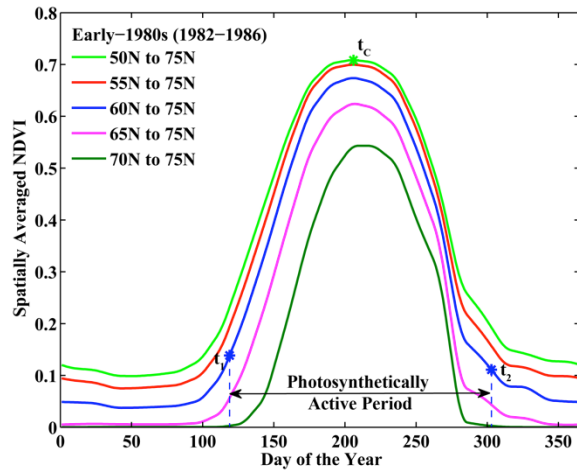
b

c
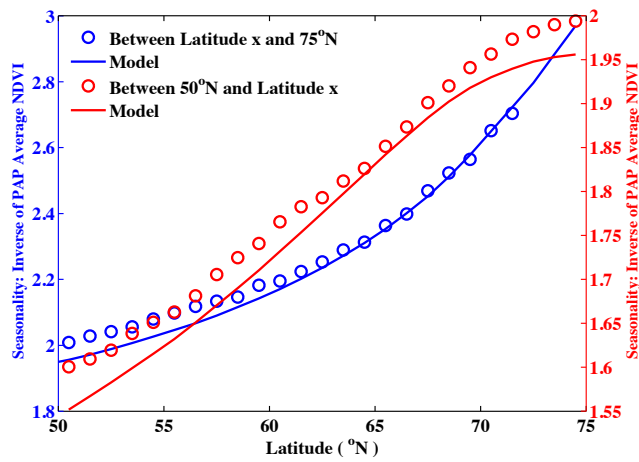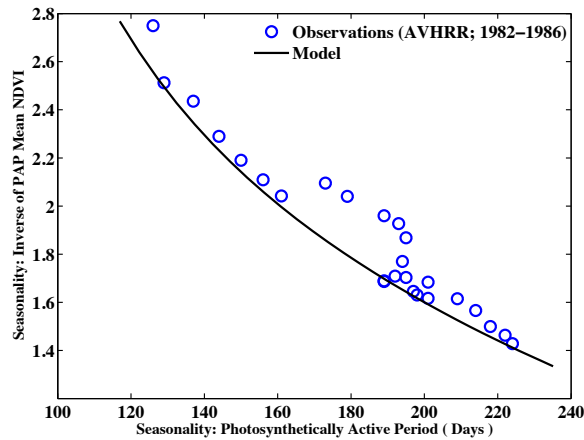
Supplementary Figure S4 | Model testing of seasonality of vegetation photosynthetic activity using NDVI. a, Annual course of NDVI over different zones bounded by L_1^oN and L_2^oN, where L_2^oN $> L_1^o$N, holding L_2^oN constant and varying L_1^oN to produce a range of seasonalities. The date of annual maximum NDVI is shown as t_C. The duration of PAP is estimated from the ground-state freeze/thaw data (Supplementary Information S2.B). **b**, Comparison of modeled and observed vegetation seasonality, both integrated between latitudes x (x-axis) and 75°N, i.e.

6

between boundaries x and 75°N (blue color; left y-axis). A similar comparison, but for latitudinal zones with boundaries 50°N and x (x-axis), is shown in red color (right y-axis). The NDVI data (Supplementary Information S1.A) are averages over the years 1982 to 1986. **c**, Comparison of vegetation seasonality defined as $[1 \div \overline{N}(l)]$ with "growing season" defined as the Full Width at Sixth of Maximum of the zonally averaged NDVI profile at the same latitude l (Supplementary Information S2.A.2).
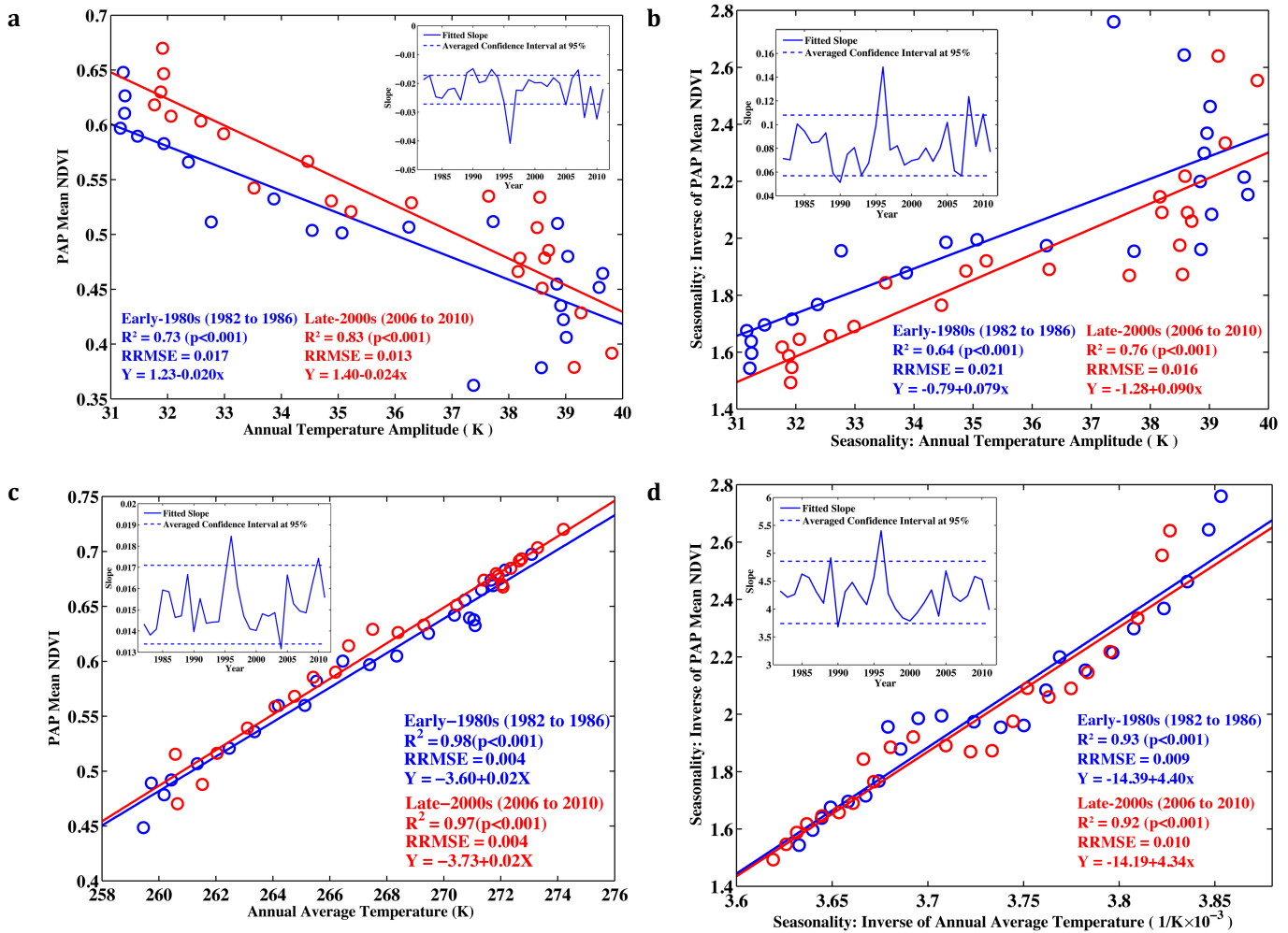
Supplementary Figure S5 | Evaluation of conventional definition of seasonality (annual temperature amplitude) and the new definition introduced in this article (inverse of annual average temperature) in terms of their relationship to vegetation photosynthetic activity expressed as PAP-mean NDVI (PAP: Photosynthetically Active Period as in the article) at the zonal scale. The annual average temperature is more closely related to PAP-mean NDVI than the annual temperature amplitude (**c** *vs.* **a**) because the former is based on the entire annual cycle of temperature while the latter is based on just two values – maximum and minimum temperatures. For the same reason, the new definition of temperature seasonality is more closely related to vegetation seasonality than the conventional definition of temperature seasonality (**d** *vs.* **b**). Similarly, the new definition of temperature seasonality is more closely related to PAP-mean NDVI than the conventional definition of temperature seasonality (not shown for brevity). The wording "more closely related to" is based on the relative root mean square error (RRMSE) of the fit, evaluated as

$$RRMSE = \sqrt{\frac{1}{n}\sum_{j=1}^{n}\left(\frac{\hat{Y}_j - Y_j}{Y_j}\right)^2} = \frac{RMSE}{\sqrt{\sum_{j=1}^{n}Y_j^2}}$$

where n is the sample size, Y_j is the jth observation, and $\hat{Y}_j$ is the jth predicted value. The annual average temperature differs from the temperature integrated over the year by a constant (=12, because of the monthly resolution of the temperature data set). Analogously, PAP-mean NDVI differs from NDVI integrated over the PAP by a constant (=PAP) at any given latitude. Thus, the respective variables (e.g. PAP-mean NDVI or NDVI integrated over the PAP) can be used interchangeably. The insets show year-to-year variation in the slope of the relationship between the respective variables and the dashed lines represent 95% confidence intervals. Annual time scale is chosen for temperature in this figure for simplicity. NOAA NCEP CPC temperature (Supplementary Information S1.C) and AVHRR NDVI data (Supplementary Information S1.A) over the Arctic and Boreal regions (Supplementary Fig. S1) were used.

9
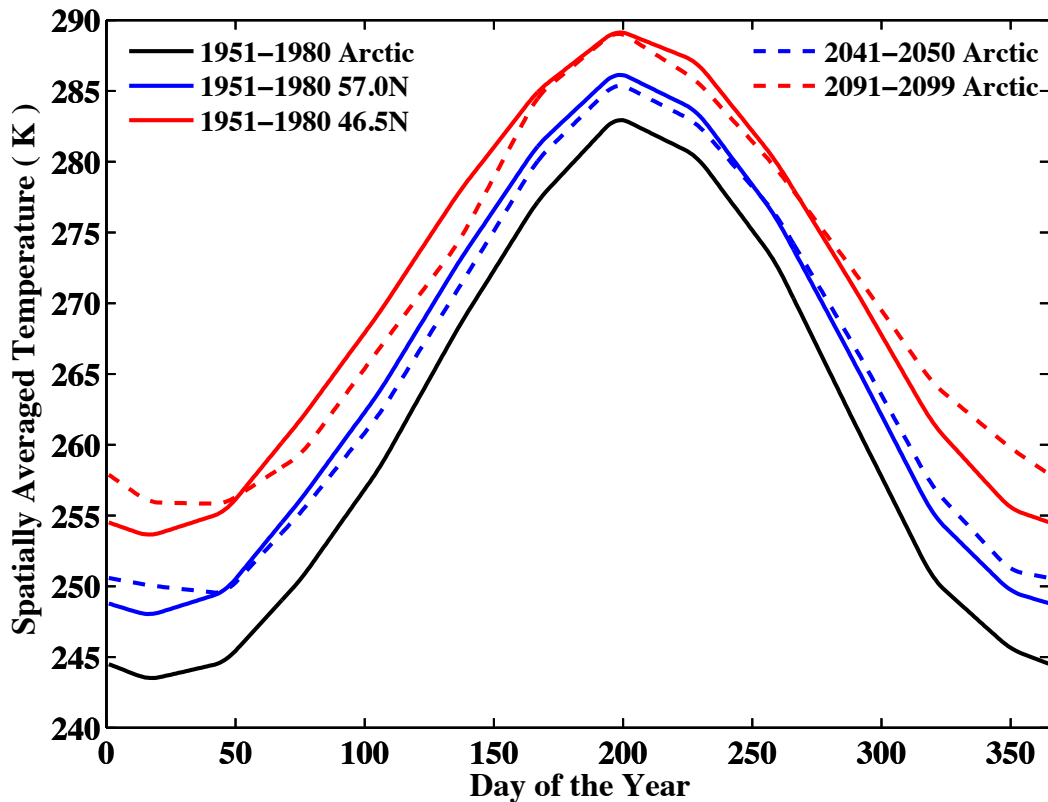
Supplementary Figure S6 | Comparison of model simulated Arctic temperature profiles for representative decades in the 21st century (dashed lines) with temperature profiles from the baseperiod (1951 to 1980) for zones >L^oN (solid lines) found through minimizing the sum of squares of differences between the two[66]. For example, the model simulated temperature profile averaged over all land areas (vegetated or barren but excluding ice sheets) north of 46.5°N during the baseperiod corresponds closest to the model simulated temperature profile of the Arctic during the period 2091 to 2099. This latitude value agrees with the latitude value found using the baseline methodology, 46.38°N (Supplementary Table S6). The baseperiod Arctic model simulation is shown for reference. The simulation is from NCAR CCSM4 model forced with RCP 8.5[30] as part CMIP5 project[4].

Trend in PAP Mean NDVI With Respect to 1982 (% Per Decade)

	<-2.0	-1.0	0.0	1.0	2.0	3.0	4.0	5.0	6.0	7.0	>8.0
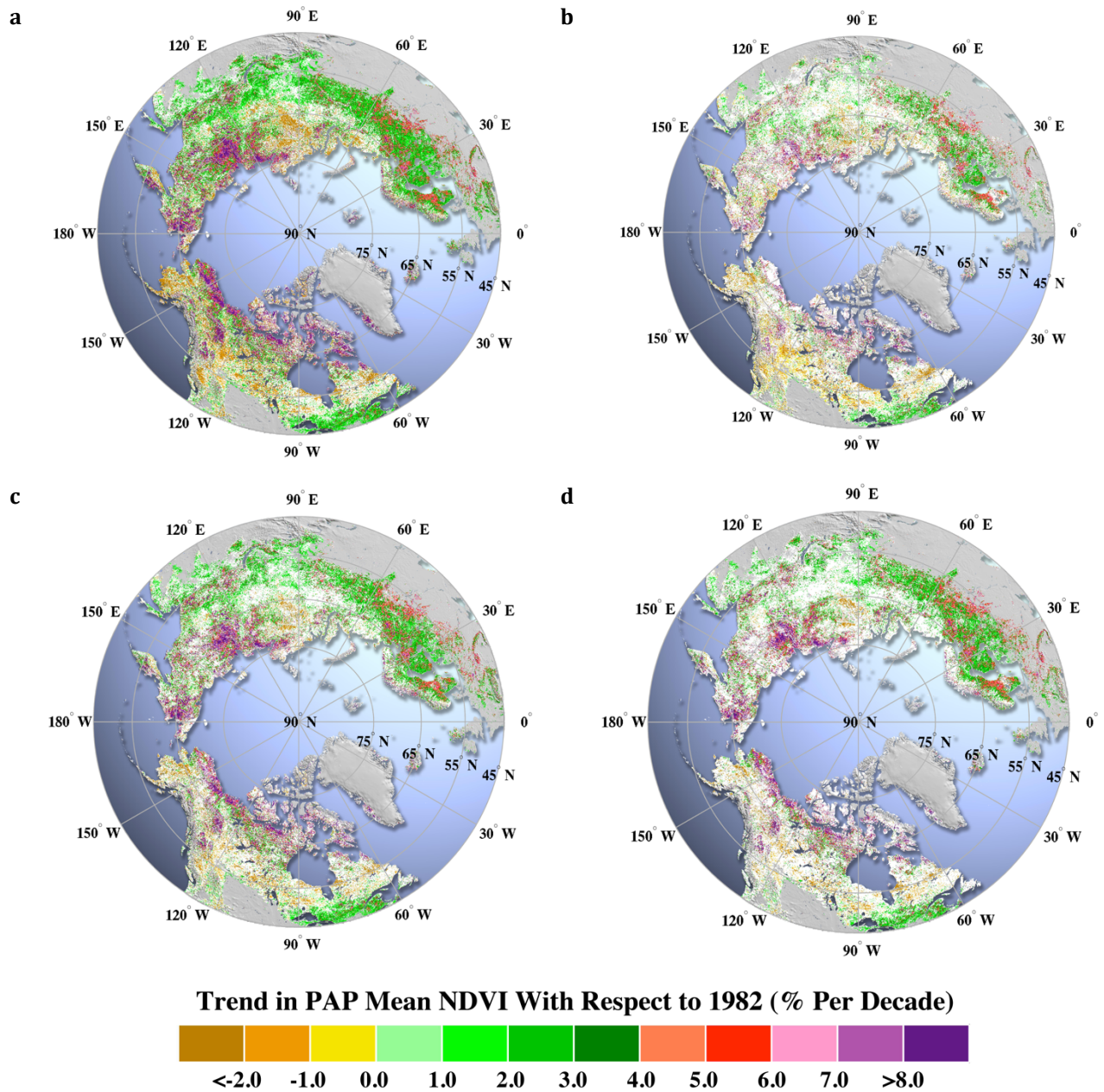
Supplementary Figure S7 | Comparison of spatial patterns of statistically significant (*p*<0.1) changes in PAP-mean NDVI from four different statistical models (Supplementary Information S2.C.1). a, Linear trend model. **b**, Auto-Regressive model of order one augmented with *p* lags. **c**, Auto-Regressive Integrated Moving Average [ARIMA(p,d,q), p=1,2; d=1; q=1, 2)]. **d**, Vogelsang's $t - PS_T$ method. Areas with statistically insignificant trends are shown in white color. Grey areas correspond to lands not considered in this study. Numerical values quantifying these changes are given in Supplementary Table S2. Companion Supplementary Table S3 presents similar results at *p*<0.05.

11
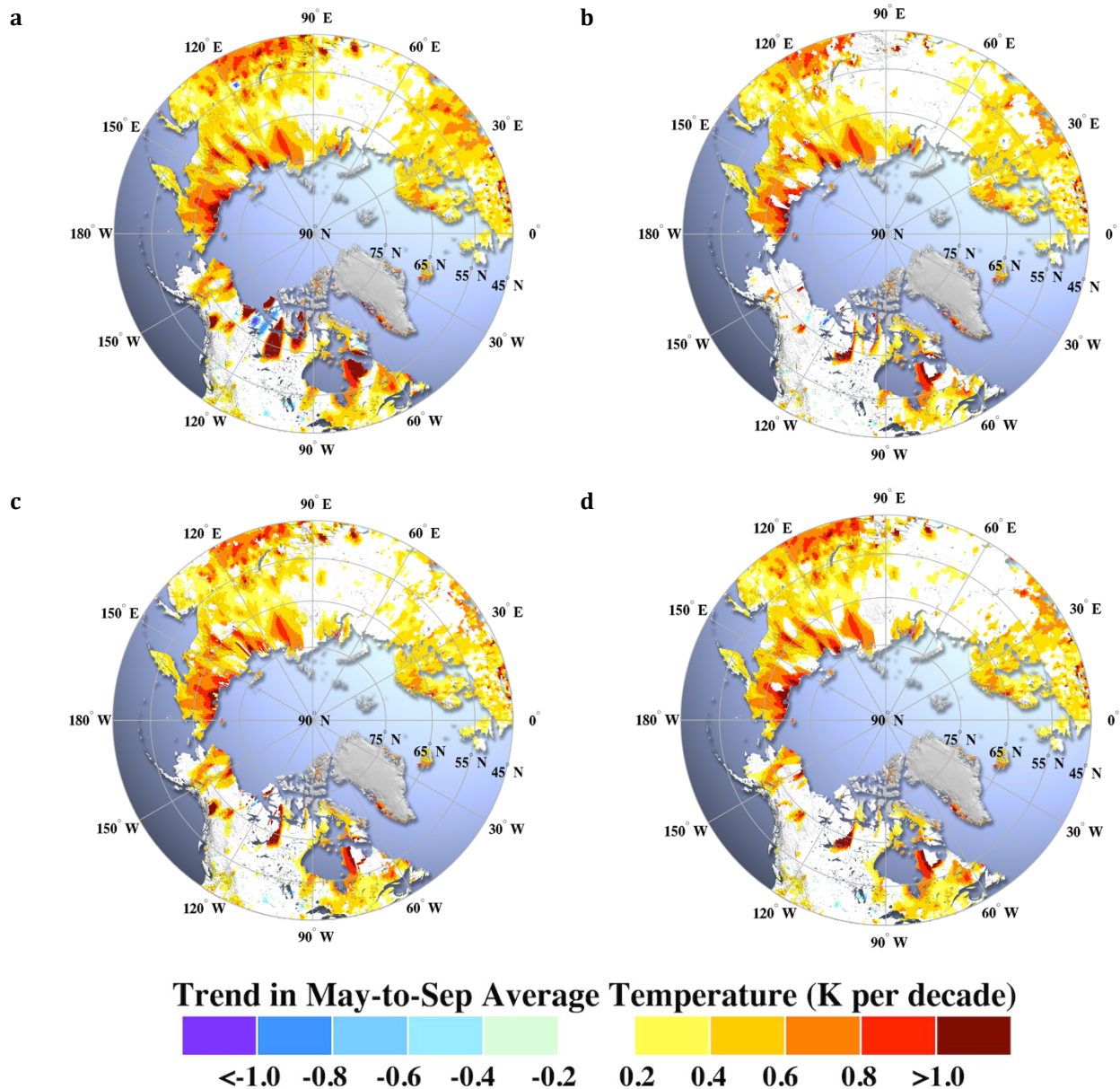
Supplementary Figure S8 | Comparison of spatial pattern of statistically significant (*p*<0.1) changes in May-to-September temperature from four different statistical models (Supplementary Information S2.C.1). a, Linear trend model. **b**, Auto-Regressive model of order one augmented with *p* lags. **c**, Auto-Regressive Integrated Moving Average [ARIMA(p,d,q), p=1,2; d=1; q=1, 2)]. **d**, Vogelsang's $t - PS_T$ method. Areas with statistically insignificant trends are shown in white color. Grey areas correspond to lands not considered in this study. The statistically significant positive ("warming") and negative ("cooling") proportions are given in Supplementary Table S4.

12
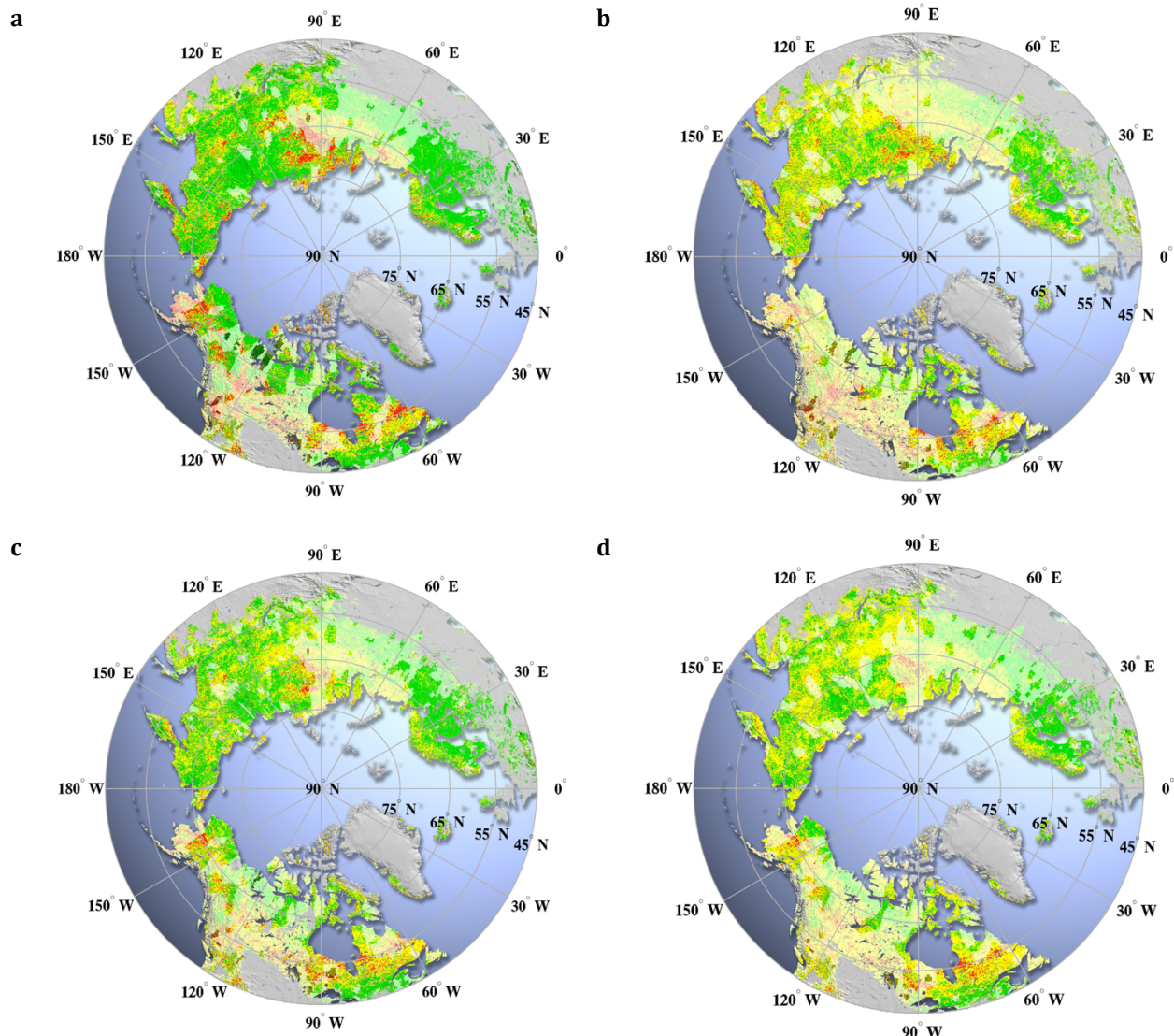
Comparison of Trends in May-to-September Temperature and PAP Mean NDVI

(-1,-1) (-1,0) (-1,+1) (0,-1) (0,0) (0,+1) (+1,-1) (+1,0) (+1,+1)

Supplementary Figure S9 | Comparison of trends of May-to-September average temperature, $\overline{T}_{WS}$, and PAP-mean NDVI, $\overline{N}_P$. a, Linear trend model. **b,** Auto-Regressive model of order one augmented with p lags. **c,** Auto-Regressive Integrated Moving Average [ARIMA(p,d,q), p=1,2; d=1; q=1, 2)]. **d,** Vogelsang's $t-PS_T$ method. Statistically significant ($p<0.1$) positive trends are denoted as +1, negative trends as -1 and insignificant trends as 0. The first character in each pair below the color bar denotes $\overline{T}_{WS}$ trend and the second character denotes $\overline{N}_P$ trend. Grey areas correspond to lands not considered in this study. Numerical values quantifying these changes are given in Supplementary Table S4. The four statistical models are described in Supplementary

Information S2.C.1. Temperature data were downscaled to the spatial resolution of NDVI data using the method of nearest neighbor interpolation. As this may potentially create artifacts, only the change in signs of trends are compared.

14

a

Trend in May to Sep Average NDVIg With Respect to 1982 (%/Decade)

<-2.0 -1.0   0.0   1.0   2.0   3.0   4.0   5.0   6.0   7.0 >8.0
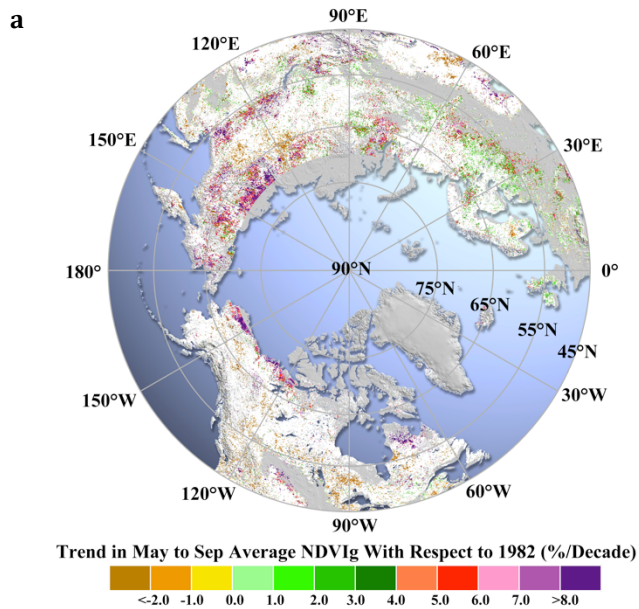
NDVIg (Earlier Version) 1982 to 2006

b

Trend in May to Sep Average NDVI3g With Respect to 1982 (%/Decade)

<-2.0 -1.0   0.0   1.0   2.0   3.0   4.0   5.0   6.0   7.0 >8.0

NDVI3g (Current Version) 1982 to 2006

c

Trend in May to Sep Average NDVI3g With Respect to 1982 (%/Decade)

<-2.0 -1.0   0.0   1.0   2.0   3.0   4.0   5.0   6.0   7.0 >8.0
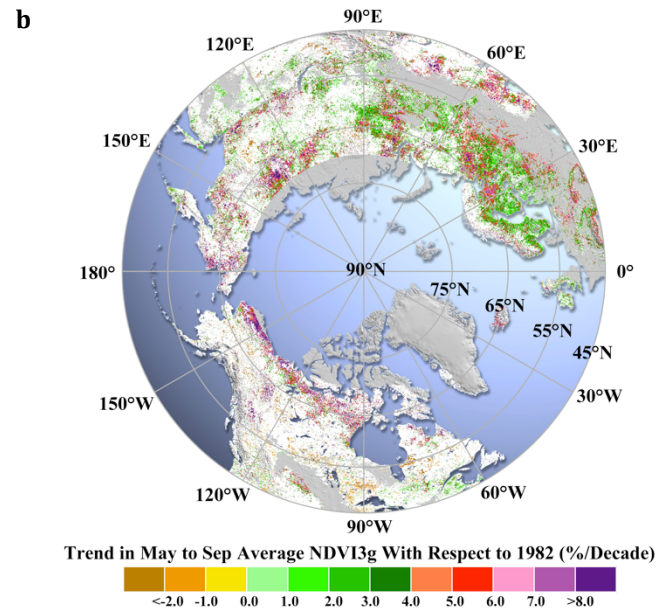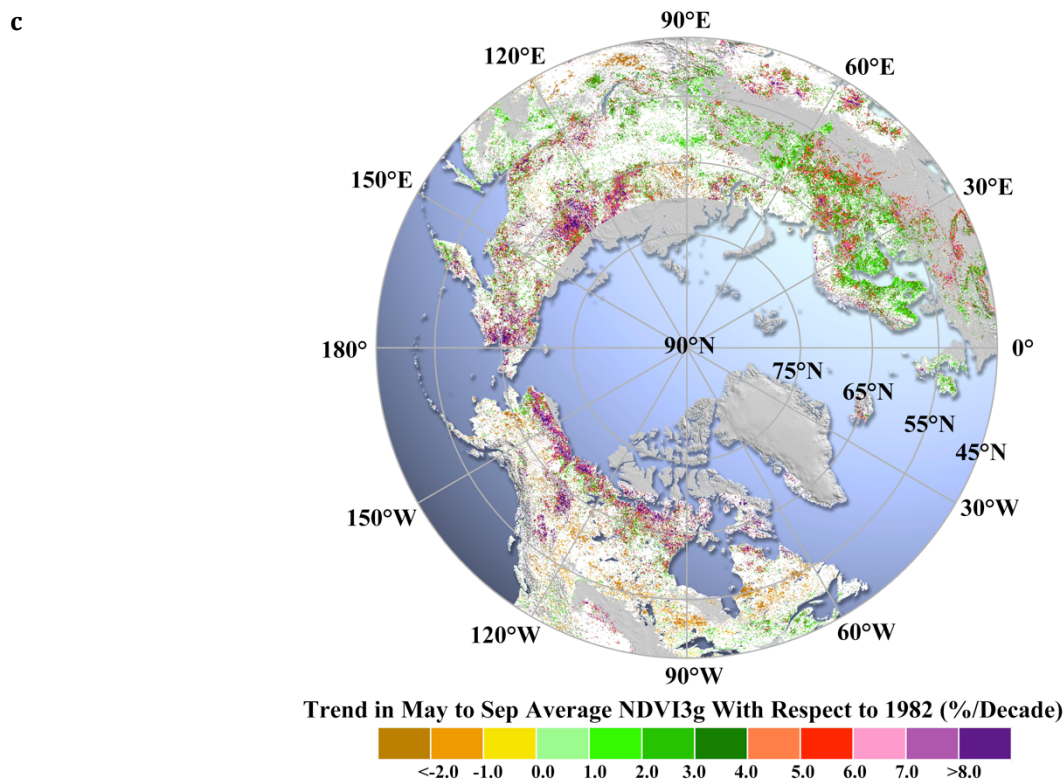
NDVI3g (Current Version) 1982 to 2011

Supplementary Figure S10 | Comparison of spatial patterns of statistically significant (p<0.1) changes in May-to-September average NDVI between an earlier version of the data set (NDVIg) and the current version used in this manuscript (NDVI3g). Statistical significance and trend estimates were determined with the Vogelsang's $t - PS_T$ method (Model 4 in

15

Supplementary Information S2.C.1). **a**, NDVIg analysis for the period 1982 to 2006. **b**, NDVI3g analysis for the period 1982 to 2006. **c**, NDVI3g analysis for the period 1982 to 2011. Areas with statistically insignificant trends are shown in white color. Grey areas correspond to lands not considered in this analysis. Numerical values quantifying these changes are given in Supplementary Tables S8 (Boreal forests with woody fraction >30%) and S9 (Boreal forests with woody fraction >40%). These results are discussed in Supplementary Information S3.A.

16

Supplementary Tables S1 to S10

Supplementary Table 1 | Vegetation classes in the Arctic and Boreal regions of this study (Supplementary Fig. S1). Vegetation classes 9 to 12 are as per the Circumpolar Arctic Vegetation Map[74]. The rest of the vegetation classes are based on the MODIS International Geosphere-Biosphere Programme (IGBP) land covers (definitions in Friedl et al.[63]).

Vegetation Class	Description
Class 1	Oceans and inland lakes
Class 2	Mixed Forests
Class 3	Deciduous Needleleaf Forests
Class 4	Evergreen Needleleaf Forests
Class 5	Forest-Shrubs Ecotone
Class 6	Closed Shrublands
Class 7	Open Shrublands
Class 8	Grasslands/Wetlands (North of Forests)
Class 9	Erect Shrub Tundra
Class 10	Prostrate Shrub Tundra
Class 11	Graminoid Tundra
Class 12	Wetlands
Class 13	Other Vegetation (e.g. crops) Not Considered in this Study
Class 14	Barren

Supplementary Table S2 | Changes in Photosynthetically Active Period (PAP) mean NDVI ($\overline{N}_P$) estimated with four statistical models (Supplementary Information S2.C.1). Greening (Browning) indicates areas showing statistically significant (p<0.1) increase (decrease) in $\overline{N}_P$. Results from Model 3 are shown in Fig. 2a. Results from all models are shown in Supplementary Fig. S7 for comparison. The Arctic and Boreal regions are shown in Supplementary Fig. S1.

Item	Model	Region	Greening (%)	Browning (%)	No-Change (%)	Invalid Data (%)
	Model 1: Linear Trend Model					
1	$y_t = \alpha + \beta t + \varepsilon_t$	Arctic	51.0	11.3	35.1	2.6
		Boreal	51.2	9.4	39.3	0.2
		Total	51.1	10.0	38.0	0.9
	Model 2: AR(1) Augmented with p Lags					
2	Step-One: $\Delta y_t = \alpha + \beta t + (\gamma - 1)y_{t-1} + \sum_{i=1}^{p} \varphi_i \Delta y_{t-i} + \varepsilon_t$	Arctic	24.5	5.5	67.4	2.6
		Boreal	25.7	8.0	66.2	0.2
	Step-Two: $\Delta y_t = \alpha + \sum_{i=1}^{p} \varphi_i \Delta y_{t-i} + \varepsilon_t$	Total	25.3	7.2	66.6	0.9
	Model 3: Auto-Regressive Integrated Moving Average [(p,d,q); p=1, 2; d=1; q=1, 2]					
3	$\Delta y_t = \alpha + \varepsilon_t + \sum_{i=1}^{p} \varphi_i \Delta y_{t-i} + \sum_{i=1}^{q} \theta_i \varepsilon_{t-i}$	Arctic	39.4	4.4	51.5	4.7
		Boreal	41.0	5.4	50.7	2.8
		Total	40.6	5.1	51.0	3.3
	Model 4: Vogelsang's $t - PS_T$ Method					
4	Vogelsang's $t - PS_T$ Method	Arctic	32.3	2.1	63.1	2.6
		Boreal	34.0	3.6	62.2	0.2
		Total	33.6	3.1	62.4	0.9

Supplementary Table S3 | Same as Supplementary Table S2 except that the statistical significance level $p<0.05$.

Item	Model	Region	Greening (%)	Browning (%)	No-Change (%)	Invalid Data (%)
Model 1: Linear Trend Model						
1	$y_t = \alpha + \beta t + \varepsilon_t$	Arctic	46.8	9.2	41.5	2.6
		Boreal	45.8	7.5	46.6	0.2
		Total	46.1	8.0	45.0	0.9
Model 2: AR(1) Augmented with p Lags						
2	Step-One: $\Delta y_t = \alpha + \beta t + (\gamma - 1)y_{t-1} + \sum_{i=1}^{p} \varphi_i \Delta y_{t-i} + \varepsilon_t$	Arctic	21.1	3.7	72.6	2.6
		Boreal	20.5	6.1	73.3	0.2
	Step-Two: $\Delta y_t = \alpha + \sum_{i=1}^{p} \varphi_i \Delta y_{t-i} + \varepsilon_t$	Total	20.7	5.3	73.1	0.9
Model 3: Auto-Regressive Integrated Moving Average [(p,d,q); p=1, 2; d=1; q=1, 2]						
3	$\Delta y_t = \alpha + \varepsilon_t + \sum_{i=1}^{p} \varphi_i \Delta y_{t-i} + \sum_{i=1}^{q} \theta_i \varepsilon_{t-i}$	Arctic	34.2	3.1	58.0	4.7
		Boreal	35.7	4.1	57.3	2.8
		Total	35.3	3.8	57.5	3.4
Model 4: Vogelsang's $t - PS_T$ Method						
4	Vogelsang's $t - PS_T$ Method	Arctic	18.5	0.7	78.2	2.6
		Boreal	20.9	1.4	77.5	0.2
		Total	20.1	1.2	77.8	0.9

3

Supplementary Table S4 | Comparison of changes in May-to-September (warm-season) temperature ($\overline{T}_{WS}$) and PAP-mean NDVI ($\overline{N}_P$). These results are shown as color maps in Figs. 3a (Model 3), 3b (Model 4) and Supplementary Fig. S9 (all models). The notation is as follows: M1 through M4 represent the four statistical models (Supplementary Information S2.C.1) used to estimate statistically significant ($p<0.1$) positive (+ve) and negative trends (-ve) trends in $\overline{T}_{WS}$ and $\overline{N}_P$. "None" indicates no statistically significant changes. Warming (Cooling) indicates statistically significant ($p<0.1$) increase (decrease) in $\overline{T}_{WS}$ (Supplementary Fig. S8). Greening (Browning) indicates statistically significant ($p<0.1$) increase (decrease) in $\overline{N}_P$ (Supplementary Fig. S7 and Supplementary Table S2). The Arctic and Boreal regions are shown in Supplementary Fig. S1. NOAA NCEP CPC temperature data were used in this analysis.

Trend		Arctic				Boreal				Total			
$\overline{T}_{WS}$	$\overline{N}_P$	M1	M2	M3	M4	M1	M2	M3	M4	M1	M2	M3	M4
Agreement													
+ve	**+ve**	36.44	14.80	24.85	17.45	34.77	14.61	25.16	18.95	35.29	14.67	25.06	18.48
-ve	**-ve**	0.15	0.04	0.01	0.00	0.20	0.23	0.14	0.04	0.19	0.17	0.10	0.03
None	**None**	11.91	31.42	19.89	32.44	16.03	36.60	22.16	28.17	14.75	34.99	21.46	29.50
Disagreement													
+ve	**-ve**	5.96	2.74	2.01	0.52	3.81	2.01	2.20	1.45	4.48	2.24	2.14	1.16
-ve	**+ve**	1.66	0.19	0.17	0.00	0.28	0.09	0.11	0.06	0.71	0.12	0.13	0.04
No Change in May-to-September Temperature													
None	**+ve**	11.30	9.09	11.36	14.41	15.86	10.90	14.84	14.95	14.44	10.34	13.76	14.78
None	**-ve**	4.36	2.57	2.17	1.48	5.27	5.68	2.90	2.05	5.07	4.72	2.68	1.87
No Change in PAP Mean NDVI													
+ve	**None**	21.25	32.53	27.57	27.72	22.49	28.40	26.30	33.12	22.10	29.69	26.69	31.44
-ve	**None**	0.69	0.56	0.14	0.00	0.47	0.64	0.49	0.39	0.54	0.61	0.38	0.27
Significant Trends													
Warming		63.65	50.07	54.43	45.69	61.07	45.02	53.66	53.52	61.87	46.60	53.89	51.08
Cooling		2.35	0.79	0.31	0.00	0.75	0.96	0.74	0.49	1.25	0.90	0.61	0.34
Greening		49.40	24.08	36.38	31.86	50.91	25.06	40.11	33.96	50.44	25.13	38.95	33.30
Browning		9.17	5.35	4.19	2.00	9.28	7.92	5.24	3.54	9.74	7.13	4.92	3.06
Invalid Data													
Invalid Data		6.02	6.06	11.84	5.98	0.82	0.82	5.70	0.82	2.44	2.45	7.60	2.43

4

Supplementary Table S5 | Regression analyses (Supplementary Information S2.C.2) **between anomalies of vegetation seasonality ($S_V = 1 \div \overline{N}_P$) and temperature seasonality ($S_T = 1 \div \overline{T}_P$) for the period 1982 to 2011**. Here $\overline{N}_P$ is Photosynthetically Active Period (PAP) mean NDVI for the Arctic or Boreal region and $\overline{T}_P$ is the corresponding PAP mean temperature. These seasonality definitions satisfy the principle that seasonality increases with latitude at an annual scale due to sun-earth geometry only. Pixels exhibiting statistically significant changes (positive and negative) in PAP mean NDVI are included in the analysis (Fig. 2a). The first row is for the Arctic region (Fig. 3c inset) and the second row is for the Boreal region (Fig. 3d inset). The 95% confidence intervals for the coefficient β_1 are given for both regression models. The Arctic and Boreal regions are shown in Supplementary Fig. S1. NOAA NCEP CPC temperature data were used in this analysis.

Y	X	$Y = \beta_0+\beta_1 X+\beta_2\text{time}+\varepsilon$			$\Delta Y = \beta_0+\beta_1\Delta X+\varepsilon$		
		R^2	β_1	t Statistic	R^2	β_1	t Statistic
S_V Arctic	S_T Arctic	0.89	2.55 (1.71, 3.39)	6.24*	0.61	2.13 (1.46, 2.80)	6.50*
S_V Boreal	S_T Boreal	0.77	2.13 (0.77, 3.49)	3.22*	0.34	1.74 (0.79, 2.68)	3.77*

*Statistically significant at $p<0.01$

Supplementary Table S6 | Historical and projected 21st century evolution of seasonality diminishment in annual temperature over the Arctic and Boreal regions. The measurements refer to temperature seasonality evaluated with CRUTEM3 data from the Climate Research Unit of the University of East Anglia, UK (Supplementary Information S1.C). The 17 coupled model simulations of historical and projected temperatures are from the Coupled Model Intercomparison Project 5 (CMIP5[4]) multi-model ensemble (Supplementary Table S7). The forcing scenario for all entries is RCP 8.5[30]. The methodology of evaluating temperature seasonality and corresponding diminishment, using NCAR CCSM4 coupled model simulated temperatures as an example, is described in Supplementary Information S2.G and shown in Fig. 4c. The temperature seasonality diminishments for three representative decades of the 21st century in this table are with respect to the base period, 1951 to 1980. The median estimates of all model projections are given in the last row. The Arctic and Boreal regions are shown in Supplementary Fig. S1.

Model	Arctic				Boreal			
	1951-1980	2001-2010	2041-2050	2091-2099	1951-1980	2001-2010	2041-2050	2091-2099
Measurements	65.27	-4.48	-	-	47.16	-4.63	-	-
BCC-CSM1.1	65.21	-7.51	-11.82	-22.46	46.12	-6.15	-10.85	-20.82
CanESM2	65.06	-5.10	-12.07	-26.58	44.79	-5.51	-14.12	-26.60
CCSM4	65.02	-3.64	-7.98	-18.64	45.02	-3.51	-10.45	-21.03
CNRM-CM5	64.78	-2.93	-8.63	-19.89	45.49	-2.92	-8.67	-19.85
CSIRO-Mk3.6	64.77	-2.13	-5.27	-14.24	44.00	-2.47	-6.90	-17.48
GFDL-CM3	64.90	-4.61	-18.35	-37.89	45.22	-4.59	-15.98	-29.47
GISS-E2-R	64.65	-3.07	-7.98	-12.75	45.17	-3.00	-7.51	-14.21
HadGEM2-CC	65.20	-1.99	-10.86	-27.70	44.57	-2.11	-12.30	-27.00
HadGEM2-ES	65.23	-2.46	-12.01	-30.41	44.55	-2.87	-13.02	-27.59
INM-CM4	64.81	-1.19	-4.50	-16.70	45.10	-1.52	-5.49	-18.50
IPSL-CM5A-MR	64.77	-3.30	-11.99	-24.65	45.56	-3.95	-13.61	-25.29
IPSL-CM5A-LR	64.66	-4.42	-10.63	-25.53	45.32	-4.59	-14.03	-26.10
MIROC-ESM	64.56	-2.62	-12.86	-32.08	45.46	-3.18	-15.78	-30.66
MIROC-ESM-CHEM	64.55	-3.34	-12.88	-34.37	45.57	-3.17	-16.19	-33.47
MIROC5	64.96	-2.98	-7.63	-21.90	44.96	-2.87	-8.23	-20.39
MPI-ESM-LR	65.01	-4.20	-10.80	-21.98	45.92	-3.30	-9.21	-19.44
NorESM1-M	64.87	-2.31	-8.43	-20.60	44.85	-2.83	-9.64	-21.82
Median of Models	64.87	-3.07	-10.80	-22.46	45.17	-3.17	-10.85	-21.82

6

Supplementary Table S7 | Information regarding model simulations of historical and projected temperatures from the Coupled Model Intercomparison Project 5 (CMIP5[4]) **multi-model ensemble used in this study** (Fig. 4c; Supplementary Table S6). For complete "Terms of Use" please see: http://cmip-pcmdi.llnl.gov/cmip5/terms.html

Beijing Climate Center, China Meteorological Administration	BCC	BCC-CSM1.1
Canadian Centre for Climate Modelling and Analysis	CCCMA	CanESM2
National Center for Atmospheric Research	NCAR	CCSM4
Centre National de Recherches Meteorologiques / Centre Europeen de Recherche et Formation Avancees en Calcul Scientifique	CNRM-CERFACS	CNRM-CM5
Commonwealth Scientific and Industrial Research Organization in collaboration with Queensland Climate Change Centre of Excellence	CSIRO-QCCCE	CSIRO-Mk3.6
NOAA Geophysical Fluid Dynamics Laboratory	NOAA GFDL	GFDL-CM3
NASA Goddard Institute for Space Studies	NASA GISS	GISS-E2-R
Met Office Hadley Centre	MOHC	HadGEM2-CC HadGEM2-ES
Institute for Numerical Mathematics	INM	INM-CM4
Institut Pierre-Simon Laplace	IPSL	IPSL-CM5A-MR IPSL-CM5A-LR
Japan Agency for Marine-Earth Science and Technology, Atmosphere and Ocean Research Institute (The University of Tokyo), and National Institute for Environmental Studies	MIROC	MIROC-ESM MIROC-ESM-CHEM
Atmosphere and Ocean Research Institute (The University of Tokyo), National Institute for Environmental Studies, and Japan Agency for Marine-Earth Science and Technology	MIROC	MIROC5
Max Planck Institute for Meteorology	MPI-M	MPI-ESM-LR
Norwegian Climate Centre	NCC	NorESM1-M

7

Supplementary Table S8 | Comparison of changes in May-to-September (M-to-S) average NDVI of natural vegetation between NDVIg (earlier version) and NDVI3g (current version and basis of this article). Abbreviation "G" in the table refers to areas showing statistically significant (p<0.1) increase in M-to-S average NDVI (Greening). Abbreviation "B" refers to areas showing statistically significant (p<0.1) decrease in M-to-S average NDVI (Browning). Abbreviation "N" refers to areas showing no statistically significant changes in M-to-S average NDVI (No-change). Statistical significance was assessed using the Vogelsang $t - PS_T$ method (Model 4 in Supplementary Information S2.C.1) which was also used in previous studies[10,45,46]. Natural vegetation types in the 45°N to 70°N were included in this analysis. These vegetation classes were divided into: (1) Boreal forests with woody fraction greater than 30% and (2) Other natural vegetation. Boreal forests consisted of: Evergreen and Deciduous needleaf forests and Mixed forests. Other natural vegetation consisted of: Broadleaf forests, Closed and Open shrublands, Woody grasslands and Grasslands. Land cover types not included are: Croplands, Permanent wetlands, Cropland/Natural vegetation mosaic, Barren or sparsely vegetated, Urban and built-up, Snow and ice, Water and unclassified. The first row shows results from NDVIg for the period 1982 to 2006. The second row shows results from NDVI3g for the same period. The third row shows results from NDVI3g for the period 1982 to 2011. The area of natural vegetation with valid NDVI data (9 out of 10 positive NDVI values during M-to-S) in North America (NA), Eurasia (EA) and Circumpolar (CP) region is given in the first column. The greening, browning and no-change fractions are with respect to these areas. Boreal forest entries in parenthesis are proportions with respect to total area of Boreal forests in NA, EA and CP, respectively. Companion Supplementary Table S9 shows results for Boreal forests with woody fraction greater than 40% (as determined by the MODIS Vegetation Continuous Fields product).

NDVI Data Set (Areas in 10^6 km^2)	NORTH AMERICA						EURASIA						CIRCUMPOLAR (North America + Eurasia)					
	Boreal Forests Woody Fraction > 30%			Other Natural Vegetation			Boreal Forests Woody Fraction > 30%			Other Natural Vegetation			Boreal Forests Woody Fraction > 30%			Other Natural Vegetation		
	G (%)	B (%)	N (%)	G (%)	B (%)	N (%)	G (%)	B (%)	N (%)	G (%)	B (%)	N (%)	G (%)	B (%)	N (%)	G (%)	B (%)	N (%)
NDVIg (82-06) NA= 8.01 EA=16.46 CP=24.47	1.17 (3.06)	3.70 (9.65)	33.50 (87.29)	5.29	2.10	54.23	6.32 (17.05)	0.84 (2.27)	29.90 (80.67)	11.47	1.83	49.63	4.64 (12.37)	1.78 (4.74)	31.08 (82.89)	9.45	1.92	51.14
NDVI3g (82-06) NA= 9.72 EA=17.87 CP=27.59	1.97 (5.60)	2.17 (6.16)	31.02 (88.23)	10.27	1.42	53.15	16.37 (45.43)	0.09 (0.25)	19.58 (54.32)	17.71	0.49	45.76	11.30 (31.62)	0.82 (2.30)	23.61 (66.08)	15.09	0.82	48.36
NDVI3g (82-11) NA= 9.72 EA=17.87 CP=27.59	2.51 (7.15)	3.92 (11.15)	28.73 (81.70)	15.36	3.54	45.94	16.02 (44.44)	0.10 (0.28)	19.92 (55.29)	17.85	1.26	44.85	11.26 (31.51)	1.45 (4.05)	23.03 (64.45)	16.97	2.06	45.23

8

Supplementary Table S9 | Same as Supplementary Table S8 except that the Boreal forests are defined as having woody fraction >40%.

NDVI Data Set (Areas in 10^6 km^2)	NORTH AMERICA						EURASIA						CIRCUMPOLAR (North America + Eurasia)					
	Boreal Forests Woody Fraction > 40%			Other Natural Vegetation			Boreal Forests Woody Fraction > 40%			Other Natural Vegetation			Boreal Forests Woody Fraction > 40%			Other Natural Vegetation		
	G (%)	B (%)	N (%)	G (%)	B (%)	N (%)	G (%)	B (%)	N (%)	G (%)	B (%)	N (%)	G (%)	B (%)	N (%)	G (%)	B (%)	N (%)
NDVIg 82-06 NA= 8.01 EA=16.46 CP=24.47	0.88 (3.05)	2.87 (9.97)	24.99 (86.98)	5.59	2.94	62.74	4.73 (17.64)	0.54 (2.03)	21.53 (80.33)	13.07	2.12	58.01	3.47 (12.64)	1.30 (4.75)	22.66 (82.61)	10.62	2.39	59.56
NDVI3g 82-06 NA= 9.72 EA=17.87 CP=27.59	1.63 (6.17)	1.59 (6.03)	23.16 (87.81)	10.61	2.00	61.02	11.94 (46.31)	0.04 (0.15)	13.80 (53.54)	22.14	0.54	51.53	8.30 (31.95)	0.59 (2.25)	17.10 (65.79)	18.08	1.06	54.88
NDVI3g 82-11 NA= 9.72 EA=17.87 CP=27.59	2.06 (7.81)	2.88 (10.92)	21.43 (81.27)	15.81	4.58	53.24	11.58 (44.91)	0.06 (0.22)	14.15 (54.87)	22.29	1.30	50.63	8.22 (31.64)	1.05 (4.05)	16.71 (64.31)	20.01	2.46	51.55

9

Supplementary Table S10 | Regression analysis (Supplementary Information S2.C.2) between anomalies of Photosynthetically Active Period (PAP) mean NDVI time series from NASA Terra MODIS and NOAA AVHRR sensors for the overlapping period 2000 to 2011. Pixels exhibiting statistically significant changes (positive and negative) in PAP mean NDVI in the Arctic and Boreal regions (Fig. 2a) are included in the analysis. The AVHRR and MODIS data are described in Supplementary Information S1.A and S1.B. The Arctic and Boreal regions are shown in Supplementary Fig. S1. Regression Model 2, which is based on first differences of the respective quantities, is statistically more robust than regression Model 1, which is based on level quantities (Supplementary Information S2.C.2).

Vegetation Zone	AVHRR = $\beta_0+\beta_1$MODIS$+\beta_2$time$+\varepsilon$			ΔAVHRR = $\beta_0+\beta_1\Delta$MODIS$+\varepsilon$		
	R^2	β_1	t Statistic	R^2	β_1	t Statistic
Arctic	0.56	0.68	2.46**	0.42	0.49	2.55**
Boreal	0.55	0.65	1.66	0.56	0.70	3.39*

*Statistically significant at $p<0.01$; **Statistically significant at $p<0.05$